EXPERIMENTAL APPLICATIONS OF MODAL DECOMPOSITION METHODS TO A NONUNIFORM BEAM

By

Rickey A Caldwell Jr.

A THESIS

Submitted to
Michigan State University
in partial fulfillment of the requirements
for the degree of

MASTER OF SCIENCE

Mechanical Engineering

2011

ABSTRACT

EXPERIMENTAL APPLICATIONS OF MODAL DECOMPOSITION METHODS TO A NONUNIFORM BEAM

By

Rickey A Caldwell Jr.

The goal of this research is to compute the mode shapes and in some cases the natural frequencies of a lightly damped freely vibrating nonuniform beam using sensed outputs, via accelerometers. The methods applied are reduced-ordered mass weighted proper decomposition (RMPOD), state variable modal decomposition (SVMD) and smooth orthogonal decomposition (SOD). A permutation of input impulse magnitudes, input locations, signal length, and acceleration, velocity, displacement ensembles were used in the RMPOD decomposition to gain some experience regarding the effects of input parameters and signal types on modal estimations. An analytical approximation to the modal solution of the Euler-Bernoulli beam equation is developed for nonuniform beams. In the case of RMPOD the theory is pushed into the experimental realm. For SVMD and SOD the science is also extended into the experimental realm and is additionally applied to nonuniform beams. The results of this thesis are as follows: the analytical approximation accurately predicted the mode shapes of the nonuniform beam and can accurately predict frequencies if the correct material properties are used in the computations. RMPOD extracted accurate approximations to the first three linear normal modes (LNMs) of the thin lightly damped nonuniform beam. SVMD and SOD extracted both the natural frequencies and mode shapes for the first four modes of the thin lightly damped nonuniform beam.

I would like to dedicate this achievement to my mother, Glenda Caldwell, and my sister, Kenesha Caldwell. Additionally, there are countless others too numerous to name who believed in me and gave me a chance. To name a few Ms. Flecher, Ms. Horton, Mr. Brusick, Mr. Richard Welch, Mr. David Reed, Dr. A. Wiggins, Theodore Caldwell, M.Ed., Dr. S. Shaw, Hans Larsen, Dan and Tammy Timlin, Sloan Rigas Program, AGEP and other supporters.

Finally, to all those who fought, were bitten by dogs, beaten, threaten, murdered, ridiculed, ostracized, and paid the ultimate sacrifice so that I might have the chance to pursue higher education, a million thanks; there is no way to repay my debt to you, so I honor you and the sacrifices you made for me. I truly stand on the shoulders of giants.

To Carl.

ACKNOWLEDGMENT

Thank you Dr. Brian Feeny for your guidance and support. You astutely and masterfully led me on a journey of professional and personal development, with great temperance and patience like a benevolent Zen master. That's why I call you Yoda. Additionally, I would like to thank Dr. C. Radcliffe and Dr. B. O' Kelly, without whose help I would not be writing this now.

To the land grant philosophy- a worthwhile endeavor!

This work was supported by the National Science Foundation grant number CMMI-0943219. Any opinions, findings, and conclusions or recommendations are those of the authors and do not necessarily reflect the views of the National Science Foundation.

Additional support was received from the Diversity Programs Office and the College of Engineering at Michigan State University.

TABLE OF CONTENTS

LIST OF TABLES

LIST OF FIGURES

Chapter 1

Introduction

For beams freely vibrating in their linear elastic range with small amplitudes and known initial and boundary conditions, it is effective to describe the beam's dynamics using its mode shapes, natural frequencies, and modal damping. Generally the calculus of this information is derived from the Euler-Bernoulli beam equations or more generally the Timoshenko beam equation. The most significant difference between the two beam theories is that Timoshenko beam theory allows for warping of the cross sections and shear stress in the cross sections, and Euler-Bernoulli beam theory assumes that deformations occur in bending only and that cross-sections remain plane. In order to derive the dynamics from these beam theories one needs the material properties such as mass per unit length, Young's modulus, Possion's ratio, and geometry information such as the area moment of inertia of the cross section. If one considers discrete mass systems such as mass-spring-dashpot systems, then the mass, spring, and damping matrices must be known. In both of these cases, continuous beam and discrete mass systems, one needs to know the material properties and the geometry to compute the mode shapes and natural frequencies which can then be used to compute the dynamics of

the beam, such as displacement, velocity, and acceleration.

The focus of the thesis is on decomposition methods where an engineer could capture displacement time histories or its derivatives and use that information to find the mode shapes, and in certain cases, the natural frequencies and modal damping coefficients. In particular the focus lies in experimentally applying reduced-order mass weighted proper orthogonal decomposition (RMPOD), state variable modal decomposition (SVMD), and smooth orthogonal decomposition (SOD) to a thin lightly damped freely vibrating nonuniform beam. In applying RMPOD a permutation of several experimental parameters were taken to find which conditions would yield the best mode shape estimates, when compared to the mode shapes produced by the analytical approximation. In the case of SVMD and SOD, these decomposition methods were applied to a nonuniform experimental beam for the first time and were able to extract frequency and mode shape information.

1.1 Background

Often in engineering practice, the need to know modal parameters is of great importance. Examples include the rattling of dashboard components; payload survival of a rocket; civil engineering structures, such as bridges; and architectural structures, such as skyscrapers. Vibrations in these examples can be caused from numerous things. In the dashboard example, vibrations are caused by the engine and the rolling of the tires on the road. In rockets, vibrations are caused by combustion and aero-elastic forces. Finally, in civil and architectural structures, vibrations are caused by man-made forcing, such as machinery, natural forcing, such as wind and earth quakes; or a combination of both. To determine the modal parameters of these structures, one needs to perform a modal analysis.

Linear modal analysis will yield three parameters: damping, natural frequencies, and mode shapes. Damping, when positive, is a means to take energy from the system, and damping always exists in natural systems, albeit minuscule in some cases [1]. Positive damping causes the amplitude of displacement of a freely vibrating object to diminish over time [1]. In the figure below, damping causes the vibrations to decay. Damping also limits the amplitude of oscillations during a phenomenon called resonance, which is related to the natural frequency and forcing.

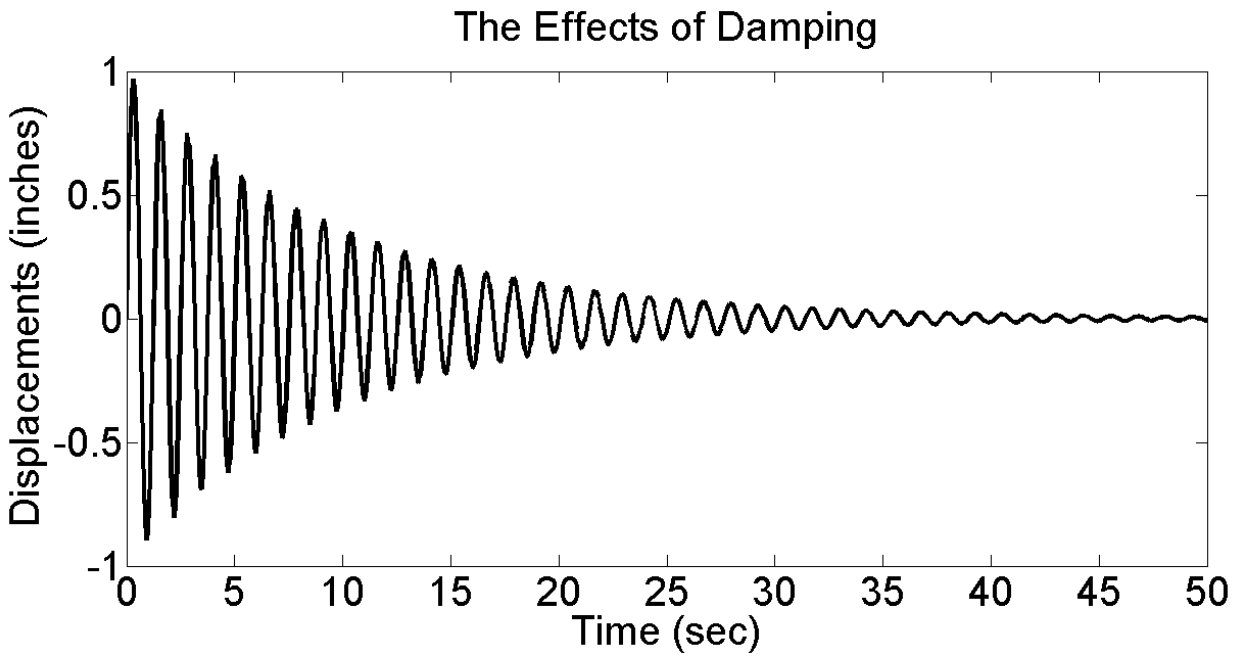

Figure 1.1: Effects of damping on free vibrations.

The natural frequencies are the frequencies in which an unforced, undamped system will vibrate. For a single degree of freedom (SDOF) system there will be one frequency ω_n. For multiple degrees of freedom or distributed parameter systems, such as a continuous beam, there are several to infinitely many natural frequencies [2]. The beam free vibration can include all of the natural frequencies simultaneously, and often the higher frequencies decay more quickly than the lower frequencies. Towards the end of the oscillations, the beam will

vibrate primarily at one frequency (typically the lowest called the fundamental frequency) [2].

When an object is being forced with harmonic excitation or random excitation and the frequency of the excitation approaches the natural frequency, a large magnification in the oscillation amplitudes will be observed. This is called resonance. For a single degree of freedom, the displacement amplitudes at resonance namely when the forcing frequency ω equals the undamped natural frequency ω_n is $X = \frac{F_0}{c\omega_n}$ where c is the damping coefficient, and F_0 is the amplitude of forcing. One can see from the equation that as c approaches zero the displacement amplitude, X, approaches infinity, and as c approaches infinity, X approaches zero. In a MDOF (multiple degree of freedom) or distributed parameter system, for each natural frequency or modal frequency, there exists a corresponding characteristic deflection called a mode shape. The lowest natural frequency is called the fundamental frequency and the corresponding mode shape is called the fundamental mode [2]. The second lowest natural frequency and mode shape are called the second natural frequency and the second mode. The same holds for the third, fourth, fifth, and so on. Usually only the first five or so natural frequencies or modes have significance in engineering practice.

Mode shapes, specifically linear normal modes, describe characteristic shapes of oscillations, where each point in the system vibrates harmonically, and all the points go through zero and extreme values simultaneously. This is called synchronous oscillation. Modes shapes represent topographical information with regard to deflections.

Damping, natural frequencies, and mode shapes collectively characterize many natural systems. In structures, such as bridges, this information will indicate how the bridges will behave under most conditions. If designed correctly, the bridge can handle many different

types of vehicles, earthquakes, and wind loads. However, if the bridge is designed without these factors in mind, disaster may occur. One such infamous bridge is the Tacoma Narrows Bridge, which high winds had aerodynamic instability that created negative damping and led to the self excitation of a torsional mode of a a bridge section at .2 Hz. The excitation of the torsional mode caused the bridge to oscillate until it fell apart [3]. Eventually, the bridge was redesigned to withstand its wind load using the information from a modal analysis [3].

There are two types of modal analysis scenarios: analytical and experimental.

1.1.1 Analytical Modal Analysis

To compute the modal parameters analytically, the governing equations of motion must be derived from the laws of physics. In linear, time-invariant systems, seeking a synchronous motion solution gives rise to an eigensystem equation which, when solved, provides modal information. The following simple example illustrates the analytical method.

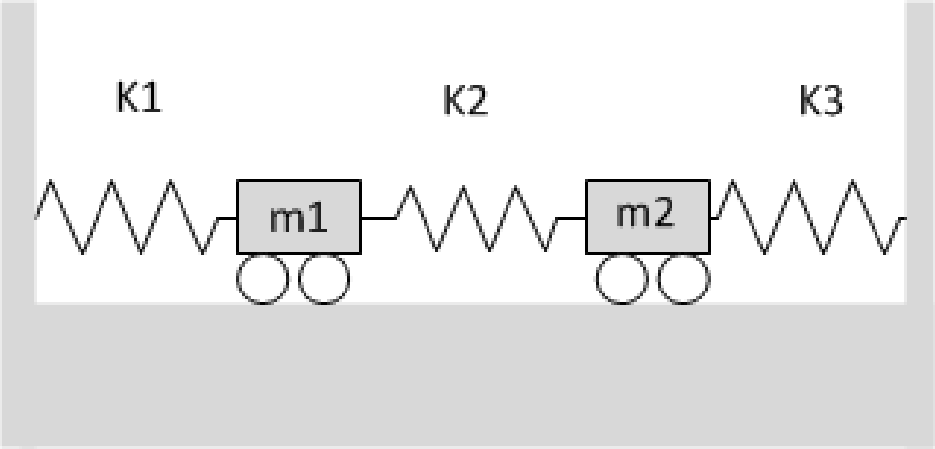

Figure 1.2: Mass-spring-dashpot (MSD) system.

For an undamped mass spring system like that illustrated in Fig 1.2 the governing equations take the form.

$$\mathbf{M}\ddot{\mathbf{x}} + \mathbf{C}\dot{\mathbf{x}} + \mathbf{K}\mathbf{x} = \mathbf{0} \tag{1.1}$$

where $\mathbf{M}$ is the mass matrix, $\mathbf{C}$ is the damping matrix, $\mathbf{K}$ is the stiffness matrix, and $\mathbf{x}$ and its derivatives are acceleration, velocity, and displacement vectors. Often the damping matrix can be assumed to be proportional to the mass and stiffness matrix such that $\mathbf{C} = \alpha\mathbf{M} + \beta\mathbf{K}$. In this case, the mode shapes of the undamped system also represent those of the damped system. We continue with the analysis for the system with $\mathbf{c} = \mathbf{0}$. A trial solution of $\mathbf{x} = \boldsymbol{\phi}\exp^{i\omega t}$ is plugged in for $\mathbf{x}$ which leads to the generalized eigenvalue problem $[-\omega^2\mathbf{M} + \mathbf{K}]\boldsymbol{\phi} = \mathbf{0}$. A solution is $\boldsymbol{\phi} = \mathbf{0}$; but this is a trivial solution. To enable nontrivial solutions, the determinant of $[-\omega^2\mathbf{M} + \mathbf{K}]$ is set equal to zero and solved for ω. The roots ω_i^2 of the characteristic equation are called eigenvalues and the corresponding $\boldsymbol{\phi}$ of each eigenvalue is called the eigenvector, and they satisfy the relationship $\mathbf{B}\mathbf{v} = \lambda\mathbf{v}$. Where $\mathbf{B} = \mathbf{M}^{-1}\mathbf{K}$, $\mathbf{v} = \boldsymbol{\phi}$, and $\lambda = \omega^2$. Using these parameters and superposition the displacements of all masses are:

$$\mathbf{x} = \sum_i c_i\boldsymbol{\phi}\sin(\omega_i t + \psi_i) \tag{1.2}$$

where c_i and ψ_i are based on the initial conditions. It can be easily seen from the above equation that the eigenvector controls the shape of oscillation of each sinusoid and the square root of the eigenvalue controls the frequency of oscillation.

In this particular example, damping was assumed to be zero (i.e. the system is operated in a vacuum and friction is ignored). Although this is a discrete system, similar methodologies

are known for continuous systems, such as a cantilevered beam which is illustrated by an example next.

The Euler-Bernoulli equation for an unforced uniform beam with boundary conditions corresponding to a cantilevered beam is:

$$\begin{aligned} m(x)\ddot{y} + \frac{d^2}{dx^2}[EI(x)\frac{d^2u}{dx^2}] &= 0 \\ y(0,t) &= 0 \\ \frac{d}{dx}[y(0,t)] &= 0 \\ \frac{d^2}{dx^2}[EI(x)y(L,t)] &= 0 \\ \frac{d^3}{dx^3}[EI(x)y(L,t)] &= 0 \end{aligned} \tag{1.3}$$

In the equation x is the axial coordinate, $m(x)$ is the mass per unit length, E is the Young's modulus, $I(x)$ is the area moment of inertia of the cross section and $y = y(x,t)$ is the transverse displacement. This is a partial differential boundary value problem and can be solved using the method of separation of variables. Plugging $y = X(x)\Gamma(t)$ leads to two equations: one in the spatial variable $X(x)$ and the other in time $\Gamma(t)$. The time equation leads to the eigenvalues and the natural frequencies of the system such that $\omega_n = \beta_n^2\sqrt{\frac{EI}{\rho}}$, where ω_n is the natural frequency. β_n are values that satisfy the following equation, $1 + \cos(\beta_n)\cosh(\beta_n) = 0$ based on boundary conditions listed above. The spatial variable leads to the generalized eigenfunction $X(x) = A\cosh(\beta x) + B\sinh(\beta x) + C\cos(\beta x) + D\sin(\beta x)$. The values of the the constants A, B, C, and D depend on the boundary conditions [2, 4].

1.1.2 Experimental Test Modal Analysis

Experimental modal analysis can be categorized in two ways: input-based where forcing is measured [5, 6]; and output-only, when only displacements, velocities, accelerations, or stresses are measured. Both types of methods have their own particular advantages. Input methods systems can fall into several different categories, including single input single output (SISO). In SISO systems, a single sensor is used at one location and a known or measured input, such as an impact hammer, is applied at one location. With SISO "modal analysis", modes cannot be determined; only natural frequencies, which is achieved by computing a fast Fourier transform on the vibration signal. Single input multiple output (SIMO) systems use multiple sensors and single measured input at one location. Other configurations exist for different testing needs. The process is the same; input measurements and output measurements are used to create a frequency response function, which is then used to gather the modal information [1].

Output-only modal analysis only uses outputs (e.g. displacements, velocities, accelerations, or stresses) to determine the modal information. This is useful when inputs cannot be recreated in the lab environment or they are unknown and cannot be measured. Other benefits include the avoidance of frequency response functions and long and cumbersome testing procedures [7]. Output-based modal analysis can be classified as time-based or frequency-based. The latter is very common in many engineering systems, e.g. in the Laplace domain in control systems. Some examples of time domain methods include the eigensystem realization algorithm [8], Ibrahim time domain method [9], independent component analysis [10, 11], and polyreference method [12]. Examples of frequency-based methods are orthogonal polynomial methods [13, 14], complex mode indicator function [15], and frequency

domain decomposition [16]. The methods that will be explored in this body of work are based on the time domain and are extensions of proper orthogonal decomposition. They include mass weighted proper decomposition, reduced-ordered mass weighted proper decomposition, smooth orthogonal decomposition, and state-variable modal decomposition. The outputs used will be displacements, velocities, and accelerations. Accelerometers were used for sensing.

1.2 Thesis Preview and Contribution

The thesis starts with Chapter Two which covers the beam experiment. This chapter describes the experimental setup, equipment used, procedures employed and the data processing. The goal of this chapter is to provide information on the data collection process.

From this point each chapter is written as a "stand-alone" module with its own development and conclusion. Chapter Three introduces the analytical approximation. The mathematical framework for the analytical approximation is reviewed in Section Two. The final section of Chapter Three ends with an example problem. Now that a method of comparison has been established the thesis moves on to the decomposition methods. Chapter Four presents the modal decomposition methods and starts with an introduction of output-only decomposition methods and proper orthogonal decomposition (POD). The first decomposition method introduced in this thesis is reduced-order mass weighted proper decomposition (RMPOD) and it is motivated from the shortcomings of POD. These shortcomings are abated by the use of a reduced-order mass matrix which is discussed next. Once the mathematical elements of RMPOD and the mass matrix are covered Section Two ends with a discussion of the experimental results when RMPOD was applied to the data. Section Three presents

SVMD and starts with a background of SVMD, followed by a summary of the mathematical development of SVMD. This section is concluded with the results of applying SVMD to the experimental beam and how this contributes the current scholarship. The last decomposition method applied in the thesis is the smooth orthogonal decomposition (SOD). Section Four starts with a background of SOD and compares it to POD. This section points to the work of Chelidze et. al. [17]. This is followed by a summary of the mathematical development of SOD. The next two subsections present the results of using SOD on the experimental data, and how this research contributes to the scholarship. Section Five juxtaposes each of these decompositions methods to each other. In the final chapter, Chapter Five concisely summarizes the conclusions reached in this research.

The contribution of this work to the scholarship primarily consists of the application of recently developed modal analysis methods to a nonuniform beam and taking prior simulations and theory in RMPOD, SVMD, and SOD to experimental applications. One example is in Yadalam et. al [18], where a rod modeled as an exponential horn is used in simulations to show that the eigenvectors of RMPOD are approximations of LNMs. This is done experimentally in this body of work by means of a nonuniform beam experiment. Additional studies include the application of a higher order derivative ensemble matrix, and the development of a testing procedure to extract "best practice methodologies" that yielded the best possible approximation to LNMs.

Chapter 2

Beam Experiment

2.1 Overview

Free vibration experiments were conducted on a tapered cantilevered beam. In the experiment a Buck Bros. tapered saw blade served as the nonuniform beam. This beam was sensed with eleven accelerometers. Specific details of the experimental setup are described in the next section. There were several experimental runs in which different experimental parameters were varied in order to gain insight on their effects on the predictions of RMPOD, SVMD, and SOD. The following sections outline the equipment used, how the equipment was configured, the data acquisition process, and the data processing.

2.2 Experimental Setup and Procedure

The saw blade handle was removed and additional holes were punched in the blade for mounting purposes. The blade was cleaned with soap, water, and a scrubbing pad to remove any oil and dirt. Next, the beam was marked and hatched to indicate the cantilevered end and the area to be clamped by the steel retaining blocks. The beam was clamped in a fixture such that the length was 11.5 inches. The width was 3.5 inches at the clamped end; tapering from 3.5 inches at a location of 1.78 inches from the clamp, to 0.80 inches at the free end. The beam was clamped such that the midline of the taper was horizontal, and the flexure of the beam was in the horizontal plane.

Accelerometers were placed at one inch intervals at the midpoint of the width starting one inch from the clamped end and progressing to the free end. Each accelerometer was attached to the beam using wax. Details of the attachment locations are given in Table 2.1 and shown in Figure 2.1.

Blade Width at Sensor Locations	
Sensor Location	Beam Width (inches)
1	3.50
2	3.40
3	3.10
4	2.82
5	2.57
6	2.30
7	2.02
8	1.75
9	1.48
10	1.2
11	0.9

Table 2.1: Beam width at sensor locations.

Accelerometer calibration data are shown in Table 2.3. The sensors were plugged into

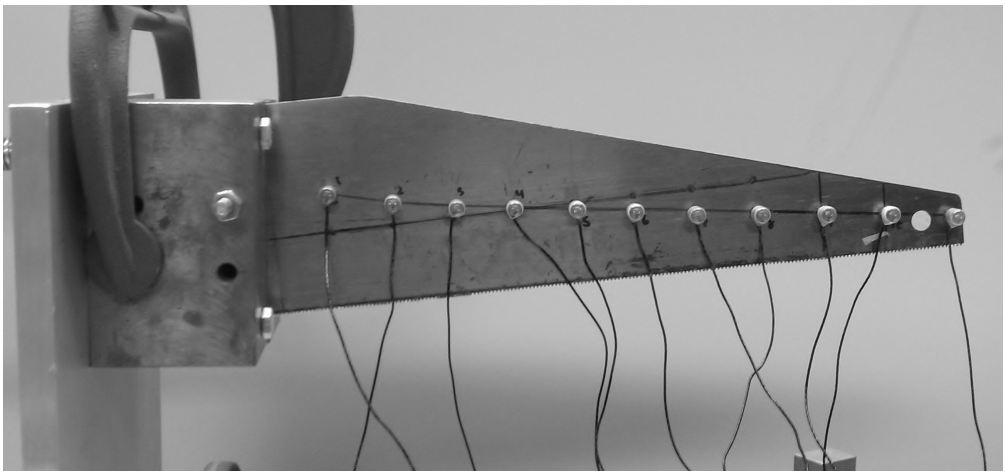

Figure 2.1: Experimental beam.

the PCB Piezotronics Model Series 481 signal conditioner and each channel had a gain of 10. The first sensor at $x = 1$ inch was plugged into channel 1, and the second sensor was plugged into channel 2, etc. The signals were then sent to the TEAC Integrated Data Recorder, which had a built-in filter. The sampling rate was 5000 Hz. The built-in filter was set as a 2000 Hz low-pass filter to prevent aliasing. The highest frequency of interest was 700 Hz. A fast Fourier transform (FFT) of any of the acceleration signals during free vibration revealed the following natural frequencies: 8.45 Hz, 40.28 Hz, 107.4 Hz, 205.1 Hz, 498 Hz, and 677.5 Hz. After the data was acquired it was viewed with TEAC GX-View software. This data was saved in ASCII format and exported to Matlab for data processing. The path of the signal was accelerometer, signal conditioner, data recorder, and finally to storage in an ASCII .txt file. An equipment list is included in Table 2.2. All data acquisition equipment was turned on for five minutes prior to any data collection to allow any possible transients to die out. After the equipment had "warmed-up" the experiment was started.

The beam was lightly tapped with an impact hammer such that resulting oscillations produced voltages less than ± 1V for each accelerometer, and again with an output of less

than ±5V for each accelerometer. The beam was struck at locations $x = 2$, $x = 6$, and $x = 11$ inches from the cantilevered end.

Equipment List	
Signal Conditioner	PCB Piezotronics Model Series 481
Data Recorder	TEAC Integrated Recorder GX-1
Attachment Medium	Wax
Beam	Buck Bros. saw blade
Accelerometers	PCB Accelerometers model 352B10 (11)
	Cantilever Beam Rig

Table 2.2: Equipment list.

2.3 Additional Data Processing

The resulting accelerations were recorded and imported into MathWorks' Matlab. In Matlab further signal processing was performed. The data was truncated so that data prior to the impact were removed. The data was inspected to ensure that the maximum and minimum values of the oscillations were not saturated. The raw acceleration data was converted into $\frac{in}{sec^2}$ using the conversion factors in Table 2.3. The means of the acceleration signal were removed. Since the accelerometers had phase distortions near 8 Hz, a high-pass filter was used with a cutoff frequency of 20 Hz. Filtering was done using Matlab's "lsim" function with the acceleration data as input to the transfer function

$$G(s) = \frac{s^2}{s^2 + 20\pi\sqrt{2}s + (20\pi)^2}. \tag{2.1}$$

This attenuated the first mode and consequently removed the first mode from the results of the decomposition methods. Within Matlab the mean of each signal was again subtracted. The signal was passed through this second-order high-pass filter twice: once forward and

the second time backwards, to correct the phase shifting that resulted from filtering. The signal was then integrated using the "cumtrapz" function in Matlab, which approximates the integral using the trapezoid rule. One iteration of this process yielded velocities. The filtering and integration process was repeated again to produce displacements. Accelerations, velocities, and displacements were used to create ensemble matrices for RMPOD, SVMD, and SOD.

All results shown in this thesis used the following input parameters: a small impulse (as defined earlier in this chapter), the beam was struck at $x = 2$ inches, and a sample window of $t = [1/4L_S\ 1/2L_S]$ where L_S is the signal length, was used.

Accelerometer Calibration Data			
Sensor Location	Serial Number	$\frac{mV}{\frac{m}{s^2}}$	$\frac{mV}{g}$
1	106257	1.044	10.24
2	94899	1.038	10.16
3	106264	1.041	9.95
4	106241	1.030	10.10
5	94860	1.063	10.43
6	94858	1.022	10.02
7	94861	1.051	10.31
8	94863	1.036	10.61
9	94905	1.059	10.39
10	94906	1.054	10.33
11	106273	1.028	10.08

Table 2.3: Accelerometer calibration data.

Chapter 3

Analytical Approximation

3.1 Motivation

As the experimental modal analysis results were obtained, the need to compare them to analytical modal parameters became necessary. Using the uniform Euler-Bernoulli beam equation was not adequate because one of the assumptions of the model is constant cross-sectional area. An analytical approximation to the nonuniform Euler-Bernoulli beam was developed and is outlined in this chapter.

3.2 Development

Since the experimental beam is a thin, lightly damped, freely vibrating beam, the governing equation can be described by the following partial differential equation and boundary

conditions:

$$
\begin{aligned}
m(x)\ddot{y}(x,t) + \frac{d^2}{dx^2}[EI(x)\frac{d^2}{dx^2}y(x,t)] &= 0 \qquad (3.1)\\
y(0,t) &= 0\\
\frac{d}{dx}[y(0,t)] &= 0\\
\frac{d^2}{dx^2}[EI(x)y(L,t)] &= 0\\
\frac{d^3}{dx^3}[EI(x)y(L,t)] &= 0
\end{aligned}
$$

It is prudent to note that the equation (3.1) was derived assuming that bending alone contributes to the strain energy and shear is neglected. Additionally, the contribution of the mass moment of inertia to the kinetic energy is ignored. Letting $y(x,t) = \Gamma(t)u(x)$ and inserting into the governing partial differential equation (3.1) leads to the following sequence of expressions:

$$
\begin{aligned}
m(x)\ddot{\Gamma}(t)u(x) + (EI(x)u''(x)\Gamma(t))'' &= 0\\
m(x)\ddot{\Gamma}(t)u(x) + \Gamma(t)(EI(x)u''(x))'' &= 0\\
m(x)\ddot{\Gamma}(t)u(x) &= -\Gamma(t)(EI(x)u''(x))''\\
\frac{\ddot{\Gamma}(t)}{\Gamma(t)} &= -\frac{\Big(EI(x)u''(x)\Big)''}{u(x)m(x)}
\end{aligned}
$$

The last expression is true only if both sides of the equation are equal to some constant, say β, which is defined as $\beta = -\omega^2$. Then:

$$\frac{\ddot{\Gamma}(t)}{\Gamma(t)} = -\omega^2 \text{ (time equation)}$$

$$(EI(x)u''(x))'' = \omega^2 u(x)\, m(x) \text{ (spatial equation)} \tag{3.2}$$

Equation (3.2) with its boundary conditions, $u(0) = 0$, $u'(0) = 0$, $[EI(x)u(L)]'' = 0$, and $[EI(u(L)]''' = 0$ is a differential eigenvalue problem. In the uniform case $EI(x)$ and $m(x)$ are constants, and equation (3.2) can be solved to obtain modes shapes and frequencies. However, in the nonuniform case, equation (3.2) is difficult, if not impossible, to solve in closed form. As such, we use an assumed mode analysis to estimate mode shapes and frequencies as described next. We first discretize equation (3.1) by approximating $y(x,t) \cong \sum_{i=1}^{n} q_i(t)u_i(x)$, where $u_i(x)$ are appropriately normalized assumed modal functions and $q_i(t)$ are the assumed modal coordinates. Then inserting into equation (3.1), multiplying (3.1) by $u_j(x)$, and integrating over the length leads to

$$\mathbf{M}\ddot{\mathbf{q}} + \mathbf{K}\mathbf{q} = \mathbf{0}. \tag{3.3}$$

where $\mathbf{q} = [q_1(t)\ \cdots q_n(t)]^T$ and where elements m_{ij} of $\mathbf{M}$ and k_{ij} of $\mathbf{K}$ are

$$m_{ij} = \int_0^L m(x)u_i(x)u_j(x)\, dx$$

$$k_{ij} = \int_0^L EI(x)u_i''(x)u_j''(x)\, dx \tag{3.4}$$

The discretization of $y(x,t)$ can be expressed as $\mathbf{y} \cong \mathbf{Uq}$. As such, the elements of $\mathbf{y}$ are $y_i = y(x_i,t) \cong \sum_{j=1}^{n} u_j(x_i)q_j(t)$. We can assume that there exists a discretized system of equations that approximate the original PDE as

$$\widehat{\mathbf{M}}\ddot{\mathbf{y}} + \widehat{\mathbf{K}}\mathbf{y} = \mathbf{0}, \tag{3.5}$$

such that the system matrices of (3.3) and (3.5) are related by $\mathbf{M} = \mathbf{U}^T\widehat{\mathbf{M}}\mathbf{U}$ and $\mathbf{K} = \mathbf{U}^T\widehat{\mathbf{K}}\mathbf{U}$. Assuming synchronous motion, such that $\mathbf{q}(t) = \mathbf{v}r(t)$, then $\mathbf{M\ddot{q}} + \mathbf{Kq} = \mathbf{0}$ leads to an eigenvalue problem,

$$\mu\mathbf{Mv} = \mathbf{Kv}. \tag{3.6}$$

Solving this eigenvalue problems leads to estimates $\mu_i \approx \omega_i^2$ of the modal frequencies of the beam model, and a modal matrix $\mathbf{V}$ for the system (3.3). Applying the transformation $\mathbf{q} = \mathbf{Vr}$ diagonalizes the equations (3.3). Remembering that $\mathbf{y} = \mathbf{Uq}$ and subbing $\mathbf{q} = \mathbf{Vr}$ into that equation, the following is derived: $\mathbf{y} = \mathbf{UVr}$. Therefore $\mathbf{y} = \mathbf{UVr}$ transforms (3.5) in original coordinates, to the diagonal system in $\mathbf{r}$. Then the discretized mode shapes are approximated by the columns of the new modal matrix $\mathbf{UV}$.

In application, a matrix $\mathbf{U}$ is created such that $\mathbf{U} = [\mathbf{u}_1\ \mathbf{u}_2\ \cdots\ \mathbf{u}_M]$ where $\mathbf{u}_i$'s are the discretized assumed modal functions. We then build the associated mass and stiffness matrices $\mathbf{M}$ and $\mathbf{K}$. Matrix $\mathbf{V}$ is created such that $\mathbf{V} = [\mathbf{v}_2\ \cdots\ \mathbf{v}_m]$ where $\mathbf{v}_i$'s are from the resulting eigensystem. Then, the discretized LNMs for the nonuniform beam are approximated as columns of $\mathbf{UV}$. This is demonstrated in the following example founded in the next section.

Material Property	Value
Young's Modulus (E)	190×10^9 Pascals
Density (ρ)	$7035 \ \frac{kg}{m^3}$
Height (h)	0.00066 m
Width (w)	0.08787 m $x \leq 0.0457$ m $-0.27409x + 0.1004 \ \ 0.0457 \text{ m} < x \leq 0.2921$ m
Length (L)	0.2921 m

Table 3.1: Assumed material properties for the beam.

3.2.1 Example

A thin steel saw blade was placed into a cantilever apparatus as described in Chapter Two. Assuming the material properties in Table 3.1 for the saw blade and applying the analytical approximation, results were found supporting the validity of the analytical approximation.

The density of the beam was calculated by first weighing the beam, next the height, width, and length of the beam was measured. The width was measured to the midpoint of the teeth, and the height measured was of the blade only and did not included the keft of the teeth. Next the beam was was divided into two sections, one rectangular and the other triangular. The area of these sections were computed subtracting out any holes, and this value was multiplied by the height to get the total volume. Finally, the mass and volume were used to compute density. Using the discretized assumed modes from the Euler-Bernoulli beam equation to write matrix $\mathbf{U}$, such that $\mathbf{U} = [\mathbf{u}_1 \ \cdots \ \mathbf{u}_M]$ where $x_j = (1 \text{ inch})j$ are the position of the accelerometer as given in Chapter Two and where the first twenty values of β_i are given in Table 3.2. Accounting for the mass of the accelerometers (0.7 grams per accelerometer), the mass and stiffness matrices $\mathbf{M}$ and $\mathbf{K}$ were computed using piecewise continuous functions of $EI(x)$ and $m(x)$ using equation (3.2.0.4) to account for the tapered

β_L	Value
β_1	1.87510406
β_2	4.694091133
β_3	7.854757439
β_4	10.995540734
β_5	14.137168391
β_6	17.278759532
β_7	20.420352251
β_8	23.561944901
β_9	26.703537555
β_{10}	29.84513020
β_{11}	32.98672286
β_{12}	36.12831551
β_{13}	39.26990816
β_{14}	42.41150082
β_{15}	45.5530934770
β_{16}	48.694686130
β_{17}	51.8362787842
β_{18}	54.9778714378
β_{19}	58.1194640914
β_{20}	61.261056745

Table 3.2: β_L's for assumed modes.

and rectangular sections of the beam. Then using equation (3.6) with matrices **M** and **K**, **V** was determined and its corresponding eigenvalues λ's were computed. These eigenvalues are the squares of radian natural frequencies, such that $\lambda_j = \omega_j^2$, and the product **UV** is a matrix where the columns approximate discretized mode shapes of the nonuniform beam.

The eigenvalues are shown in Table 3.3. The frequencies computed by the analytical approximation and the FFTs are consistent. The ratios between the estimated frequencies and FFTs were between 1.04 and 1.08. This could be caused by error the parameter group E/ρ, however this is likely to be small. Another source of error may be due to the stiffening due to the discretization, and the assumptions embedded in the beam model. Since the beam is wide, there may be some influence of plate characteristics. The infinite uniform 1-D plate equation is $\frac{\partial^2 w}{\partial t^2} + Dw'''' = 0$, while that of the uniform beam is $\frac{\partial^2 w}{\partial t^2} + \frac{EI}{m}u'''' = 0$. The ratio between parameter groups is $\frac{EI}{mD} = 1 - \nu^2$, where ν is Poisson's ratio, which bounds the deviation between the infinite 1-D plate and the Euler-Bernoulli beam. Using $\nu = 0.3$, this leads to an increase of about 5%, in the analytically estimated frequencies, which would increase the difference between the frequencies of the approximated model and the experiments. Hence the "plate effect" would worsen the frequency prediction.

To ensure that experimental frequencies were not due to torsional modes the accelerometers were moved to the perimeter of the beam and the beam was impacted off center. The resulting torsional modes are shown in Table 3.4. These torsional modes are within the frequency range of interest, but are not excited when the impulse is centered on the midline of the beam.

The frequencies were computed for discretizations $n = 5$, 10, 15, and 20. Table 3.5 shows the values of the natural frequencies, and its trend suggests convergence. The sequence $\{f_n\}$

as $n \to 20$ suggests an upper bound and the sequence $\{f_n\}$ converges only if there is a lower bound at some $F - \epsilon$ for a positive value of ϵ, and $\lim_{n\to\infty} f_n = F$ [19]. By computing the modal assurance criterion (MAC) values of all possible two pair combinations, $\binom{4}{2}$, it is obvious that the analytical modes shapes have converged by $n = 10$. Please refer to Table 3.6 for the MAC values.

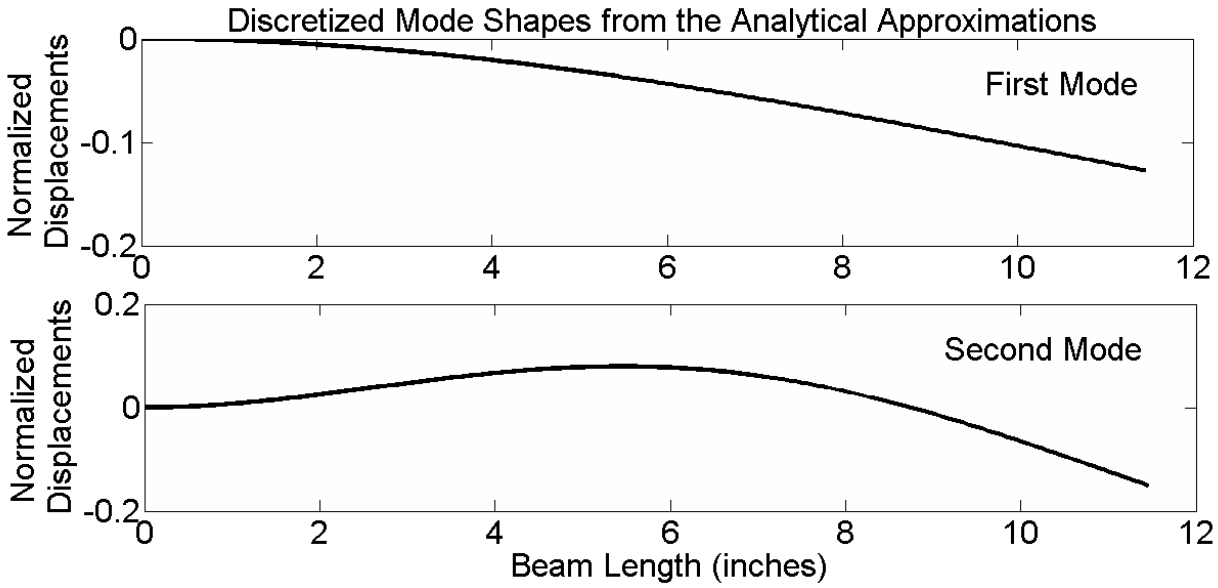

Figure 3.1: Analytical approximations of discretized mode shapes for $n = 20$, top: first mode, bottom: second mode.

Mode number	Analytical Approximation	Experimental FFT	Ratio
1	9.02 Hz	8.55 Hz	1.06
2	43.51 Hz	40.28 Hz	1.08
3	112.00 Hz	107.4 Hz	1.04
4	214.46 Hz	205.1 Hz	1.05
5	350.5 Hz	not recorded	N/A
6	520.93 Hz	498 Hz	1.05
7	725.83 Hz	677.5 Hz	1.07

Table 3.3: Comparison of natural frequencies computed from the analytical approximation compared to experimental data.

Mode number	Experimental FFT
1	226.09
2	241.17
3	386.61

Table 3.4: Torsional frequencies computed from the FFTs of the accelerometer signals.

$n = 5$	$n = 10$	$n = 15$	$n = 20$
9.02633	9.02537	9.02374	9.02135
43.52080	43.51587	43.51081	43.50646
112.27588	112.20519	112.16094	111.99878
214.94132	214.56857	214.52153	214.45728
355.84320	350.95416	350.65144	350.50359

Table 3.5: Comparison of natural frequencies for discretization values $n = 5$, 10, 15, and 20.

	Mode 1			Mode 2		
n	10	15	20	10	15	20
5	0.999	0.999	0.999	0.999	0.999	0.999
10	—	0.999	0.999	—	0.999	0.999
15	0.999	—	0.999	0.999	—	0.999
	Mode 3			Mode 4		
n	10	15	20	10	15	20
5	0.999	0.999	0.999	0.999	0.999	0.999
10	—	0.999	0.999	—	0.999	0.999
15	0.999	—	0.999	0.999	—	0.999
	Mode 5					
n	10	15	20			
5	0.9767	0.9761	0.9761			
10	—	0.999	0.999			
15	0.999	—	0.999			

Table 3.6: MAC values for two-pair combinations of n values at $n = 5$, 10, 15 and 20 for the first five modes.

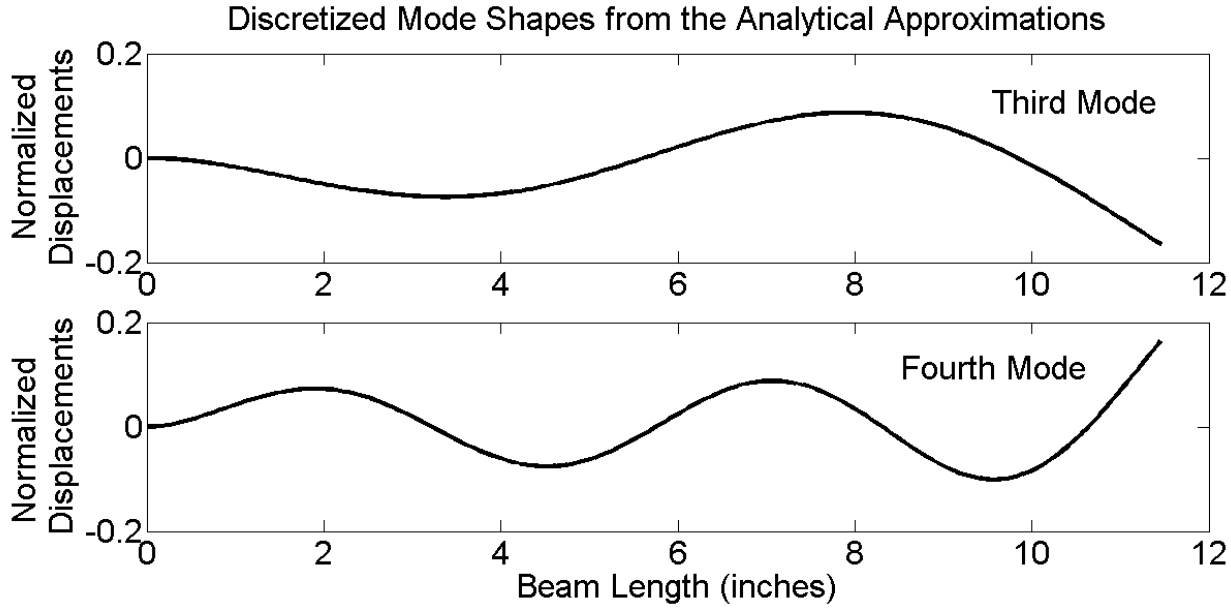

Figure 3.2: Analytical approximations of discretized mode shapes for $n = 20$, top: third mode, bottom: fourth mode.

Chapter 4

Modal Decomposition Methods

4.1 Introduction

When one needs to determine the mode shapes of a structure using time domain output-only methods there are several options including, but not limited, to proper orthogonal decomposition (POD), smooth orthogonal decomposition (SOD), state variable modal decomposition (SVMD), Ibrahim time domain method, polyreference method, and eigensystem realization algorithm [20, 12, 18, 21]. Some of these methods use sensed outputs such as displacements, velocities, or accelerations to create an ensemble matrix, followed by a correlation matrix. Then the correlation matrix is used in an eigenvalue problem. The corresponding eigenvectors generally are approximations to linear normal modes (LNMs) for lightly damped free-vibration structures. The eigenvalues, depending on the decomposition method, can approximate natural frequencies, or correspond to spectral energy densities.

One such method is the proper orthogonal decomposition (POD), which is a statisti-

cal method used to represent high degree of freedom systems in reduced-order forms and extract useful information without a loss of accuracy [22, 23]. Essentially, POD uses an eigenvalue problem (EVP) to extract a basis from an ensemble matrix consisting of sensed measurements. Berkooz et al. [23] referenced a personal communication by A.M. Yaglom which suggests that identical applications of POD were developed in different fields by different researchers. Examples include Karhunen-Loeve decomposition and principal component analysis [23, 24]. I direct the reader to pg. 542 of [23] for more details. Recently POD has been applied to the vibrations of structures in order to determine their mode shapes. In this application of POD a lightly damped freely vibrating structure is sensed with M appropriate sensors such that its displacements (typically) can be directly measured or derived (e.g. from accelerometers or strain gauges). Once the displacement time histories have been captured there will be N samples. An ensemble matrix, $\mathbf{X}$, is formed and its dimension is $M \times N$; each row corresponds to a sensor and each column is a sample time step. Thus $\mathbf{X} = [\mathbf{x}_1 \ \mathbf{x}_2 \ \cdots \ \mathbf{x}_M]^T$, where $\mathbf{x}_i = [x_i(0) \ x_i(\Delta T) \ \cdots \ x_i(N\Delta T)]$. Next, a correlation matrix, $\mathbf{R}$, is computed using $\mathbf{R} = \dfrac{\mathbf{X}\mathbf{X}^T}{N}$. The eigenvectors of $\mathbf{R}$ are approximations to linear normal modes and they are orthogonal as long as the following conditions are met: *i.* damping is small, *ii.* unforced system (freely vibrating) and *iii.* the mass matrix is uniform. Other POD schemes have been developed for cases in which these restrictions do not apply.

4.2 Reduced-order Mass Weighted Proper Decomposition

4.2.1 Motivation

Mass-weighted POD (MPOD) addresses the issue of a mass matrix that is not unity or a constant multiple of unity. In this instance a modified correlation matrix, $\widehat{\mathbf{R}}$, is formulated such that $\widehat{\mathbf{R}} = \mathbf{RM}$. If an adequate number of samples were used in the ensemble matrix the eigenvectors of $\widehat{\mathbf{R}}$ converge to the LNMs of the system $\mathbf{M}\ddot{\mathbf{x}} + \mathbf{Kx} = \mathbf{0}$ [24] given the conditions *i.* & *ii.* from above. Often in engineering practice $\mathbf{M}$ and $\mathbf{R}$ are dimensionally incongruent and the multiplication $\mathbf{RM}$ cannot be carried out. In these cases a reduced-order mass-weighted proper orthogonal decomposition can be used.

Reduced-order mass-weighted proper decomposition (RMPOD) is a potent decomposition and is very similar to POD. RMPOD employs the use of a reduced order mass matrix $\mathbf{M_r}$, such that the dimensions of $\mathbf{M_r}$ agree with the dimensions of the correlation matrix $\mathbf{R}$. A common reason the mass matrix is larger than $\mathbf{R}$ is a result of the number of sensors M available. For example the mass matrix produced by an FEA program is easily greater than 100×100. Thus by mathematical necessity in order to create a correlation matrix whose dimensions match the mass matrix the experimenter needs 100 sensors. Like with POD one senses a structure with M accelerometers. The accelerometers signals are processed to create displacements. Then an ensemble matrix $\mathbf{X}$ is created such that each row corresponds to a sensor and each column is a time step. Then $\mathbf{X} = [\mathbf{x}_1\ \mathbf{x}_2\ \cdots\ \mathbf{x}_M]^T$ with $\mathbf{x}_i = [x_i(0)\ x_i(\Delta T)\ x_i(2\Delta T) \cdots x_i(N\Delta T)]$. This ensemble matrix is used in both POD and

RMPOD, where M is the number of sensors and N is the number of time samples. (Note M is not $\mathbf{M}$, $\mathbf{M}$ is the mass matrix.)

RMPOD then uses the reduced order mass matrix $\mathbf{M_r}$ of dimension $M \times M$, such that the matrix multiplication $\mathbf{RM_r}$ is possible. Then the following problem is solved:

$$\mathbf{RM_r v} = \lambda \mathbf{v}. \tag{4.1}$$

If the damping is light, and the response is free and multimodal, the eigenvectors $\mathbf{v}$ correspond to LNMs and the eigenvalues are mass weighted mean squared of the output [18]. In summary, use of RMPOD is motivated when the mass matrix is not unity, and/or the dimensions of the mass matrix and correlation matrix is incongruent.

4.2.2 Reduced Mass Matrix of a Beam

The mass matrix is computed in much the same way it is in finite element analysis (FEA). The mass between sensors (nodes) are interpolated using, in this case, linear interpolation functions (shape functions), which accounts for the mass between sensors. The mass matrix is symmetric and can be formulated in the context of a governing equation of the form $\rho(x)\ddot{y}(x,t) + Ly(x,t) = 0$, where $\rho(x)$ is the mass per unit length and L is a linear operator. If y is discretized such that $y(x,t) = y_i = y(x_i,t)$ and $\mathbf{y} = [y_1 \ \cdots \ y_M]$, where M the is number of sensors, then interpolating between the discretized displacements yields $y(x,t) \cong \sum_{i=1}^{M} y_i \, \eta_i(x)$. The order of $\eta_i(x)$ can be chosen; in this case is $\eta_i(x)$ linear and has the form $\eta_i(x) = \frac{1}{h}(x-(i-1)h)$ for $(i-1)h \leq x < ih$, $\eta_i(x) = -\frac{1}{h}(x-(i+i)h)$ for $ih \leq x < (i+1)h$, and $\eta_i(x) = 0$ otherwise, where h is the spatial interval of the sensors on the beam. Plugging

$y(x,t) \cong \sum_{i=1}^{M} y_i\, \eta_i(x)$ into $\rho(x)\ddot{y}(x,t) + Ly(x,t) = 0$, multiplying by $\eta_j(x)$ and integrating produces the discretized system

$$\mathbf{M}_r\ddot{\mathbf{y}} + \mathbf{K}_r\mathbf{y} = 0$$

where $\mathbf{M}_r$ has the elements $\mathbf{M}_{ij} = \int_0^L \rho(x)\eta_i(x)\eta_j(x)\,dx$. For our choice of $\eta_i(x)$, we have

$$\mathbf{M}_{ij} = -\int_{ih}^{(i+1)h} \rho(x)[\frac{1}{h}(x-(i+1)h)][\frac{1}{h}(x-(j-1)h)]\,dx;\ \{i<j\ \&\ |i-j|=1$$
$$\mathbf{M}_{ij} = -\int_{jh}^{(j+1)h} \rho(x)[\frac{1}{h}(x-(i-1)h)][\frac{1}{h}(x-(j+1)h)]\,dx;\ \{i>j\ \&\ |i-j|=1$$
$$\mathbf{M}_{ii} = \int_{(i-1)h}^{ih} \rho(x)[\frac{1}{h}(x-(i-1)h)]^2\,dx + \int_{ih}^{(i+1)h} \rho(x)[\frac{1}{h}(x-(i+1)h)]^2\,dx;\ \{i=j$$

Therefore all that is needed to compute the reduced mass matrix is the interpolation functions, the mass per unit length, and h the distance between each sensor. Naturally, the dimension of the mass matrix hence the numbers of sensors affects the results: the higher the better. Once the mass matrix is computed one can implement RMPOD. To review, the computational path starts with capturing outputs from sensors, computing an ensemble matrix, and then the correlation matrix $\mathbf{R}$.

4.2.3 Experimental Results

A permutation of tap magnitudes, tap locations, signal length, and acceleration, velocity, displacement ensembles were used in the RMPOD decomposition to gain some experience regarding the effect of these parameters on RMPOD predictions. Results were evaluated using the modal assurance criterion (MAC) [25] values relative to the approximate analytical

modes as a rubric. For the RMPOD, using acceleration time signals, impacting the beam two inches for the cantilevered end, and using a time window t=[0.25s 0.5s], gave the best overall performance, although only marginally better than other permutations of the testing parameters.

For the conditions listed above, the RMPOVs (proper orthogonal values) as shown in Figure 4.1, indicating the relative mass-weighted "signal energy" associated with each extracted mode. As such, these values show some indication of modal participation and dominance. Figures 4.2, 4.3, and 4.4 show the plots of the extracted modes, modal coordinates of the extracted mode, and the FFT of the modal coordinates for the second, third, and fourth mode, respectively.

Modal coordinates were used to further evaluate the decomposition. The modal coordinates are defined through the transformation $\mathbf{A} = \ddot{\mathbf{X}} = \mathbf{V}\ddot{\mathbf{Q}}$, such that $\ddot{\mathbf{Q}}$ is an ensemble of modal acceleration time histories. The notations "$\ddot{\mathbf{X}}$" and "$\ddot{\mathbf{Q}}$" are used loosely to indicate ensembles of acceleration quantities, as oppose to the derivative of ensembles, as ensembles are merely matrices of numbers. Then the modal accelerations are given by $\ddot{\mathbf{Q}} = \mathbf{V}^{-1}\mathbf{A}$. The magnitude of the FFT of the modal coordinate acceleration for the second mode showed a single peak at 39.14 Hz. The third modal coordinate acceleration has a maximum peak at 107.6 Hz and smaller peak at 39.14 Hz. This shows some pollution from the second mode into the third modal coordinate acceleration. A similar phenomenon occurs for the fourth modal coordinate acceleration coordinate, which had a maximum peak at 205.5 Hz, followed by 39.14 Hz, and finally, 107.6 Hz. Despite this modal pollution, the extracted mode shapes

were strong approximations to the linear normal modes, which is evident by MAC values close to unity for these modes. Those values are 0.986, 0.852, and 0.912 for the second, third, and fourth modes, respectively. The estimated modes in comparison to the analytically approximated modes are shown in Figures 4.2, 4.3, and 4.4. Table 4.1 shows the MAC values between the RMPOD extracted modes and the approximate analytical modes. For instructive purposes Figure 4.5 shows an example of a poor LNM approximation by RMPOD.

Modes	RMPOD
2	0.986
3	0.852
4	0.912
5	0.915
6	0.861

Table 4.1: MAC values for RMPOD when compared to the approximate analytical modes.

4.3 State Variable Modal Decomposition

4.3.1 Background

State variable modal decomposition (SVMD) is very similar to proper orthogonal decomposition (POD) in methodology. As in POD an ensemble matrix is formed using sensed outputs. POD uses the ensemble matrix $\mathbf{X}$ consisting of sampled displacement vectors, while SVMD uses an ensemble matrix $\mathbf{Y}$ which consists of sampled velocity and displacement vectors; hence the term "state variable" [26]. As such a $2M \times N$ ensemble matrix $\mathbf{Y} = [\mathbf{y}(t_1)\ \mathbf{y}(t_2)\ \cdots\ \mathbf{y}(t_N)]$ is built, where $\mathbf{y}(t) = [\dot{\mathbf{x}}_1(t), \cdots \dot{\mathbf{x}}_M(t);\ \mathbf{x}_1(t) \cdots \mathbf{x}_M(t)]^T$ as shown in Table 4.2, where N is the number of samples and the M is the number of sensors.

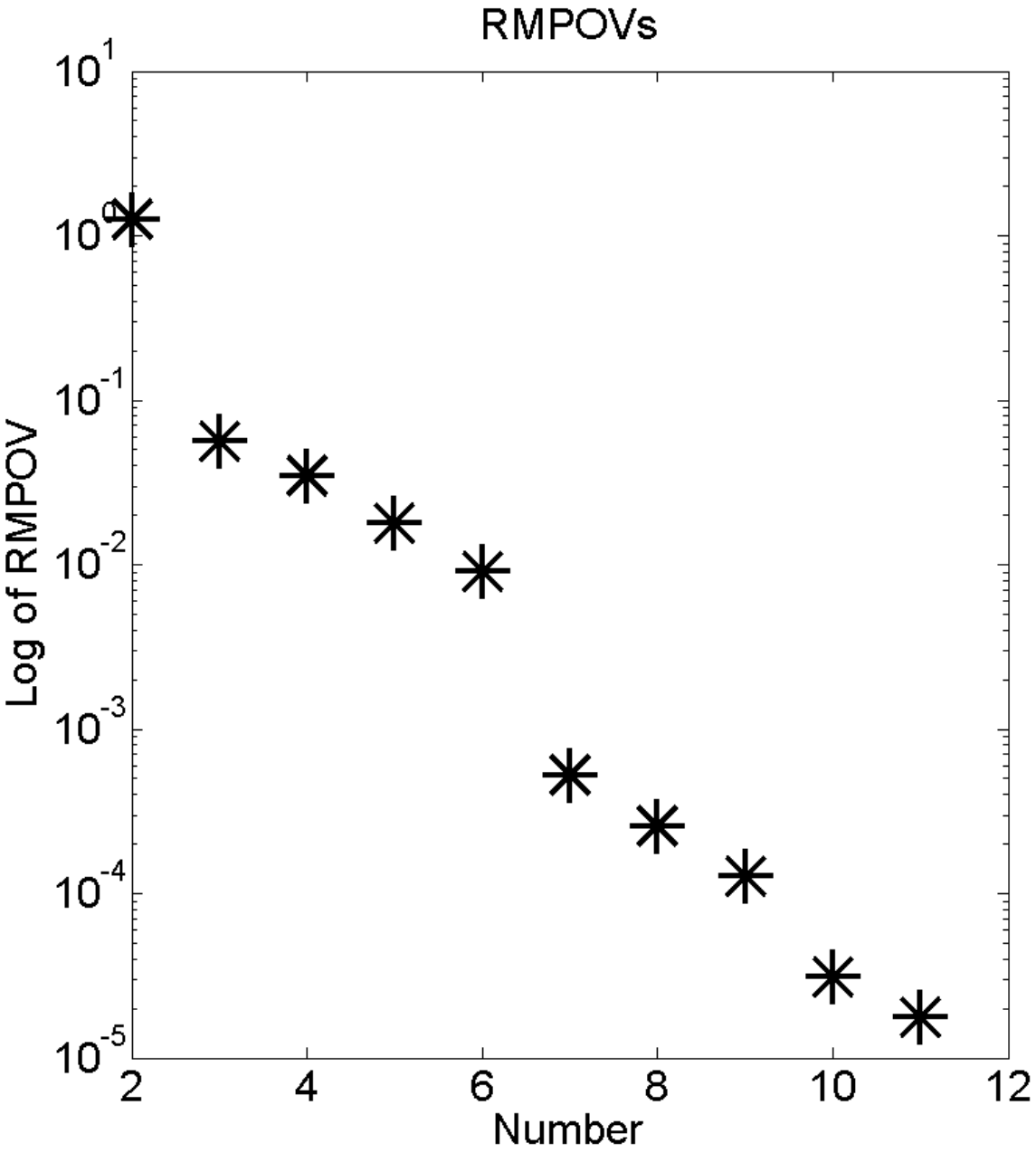

Figure 4.1: RMPOVs: mode (2) 1.2591, mode (3) 0.0562, mode (4) 0.0346.

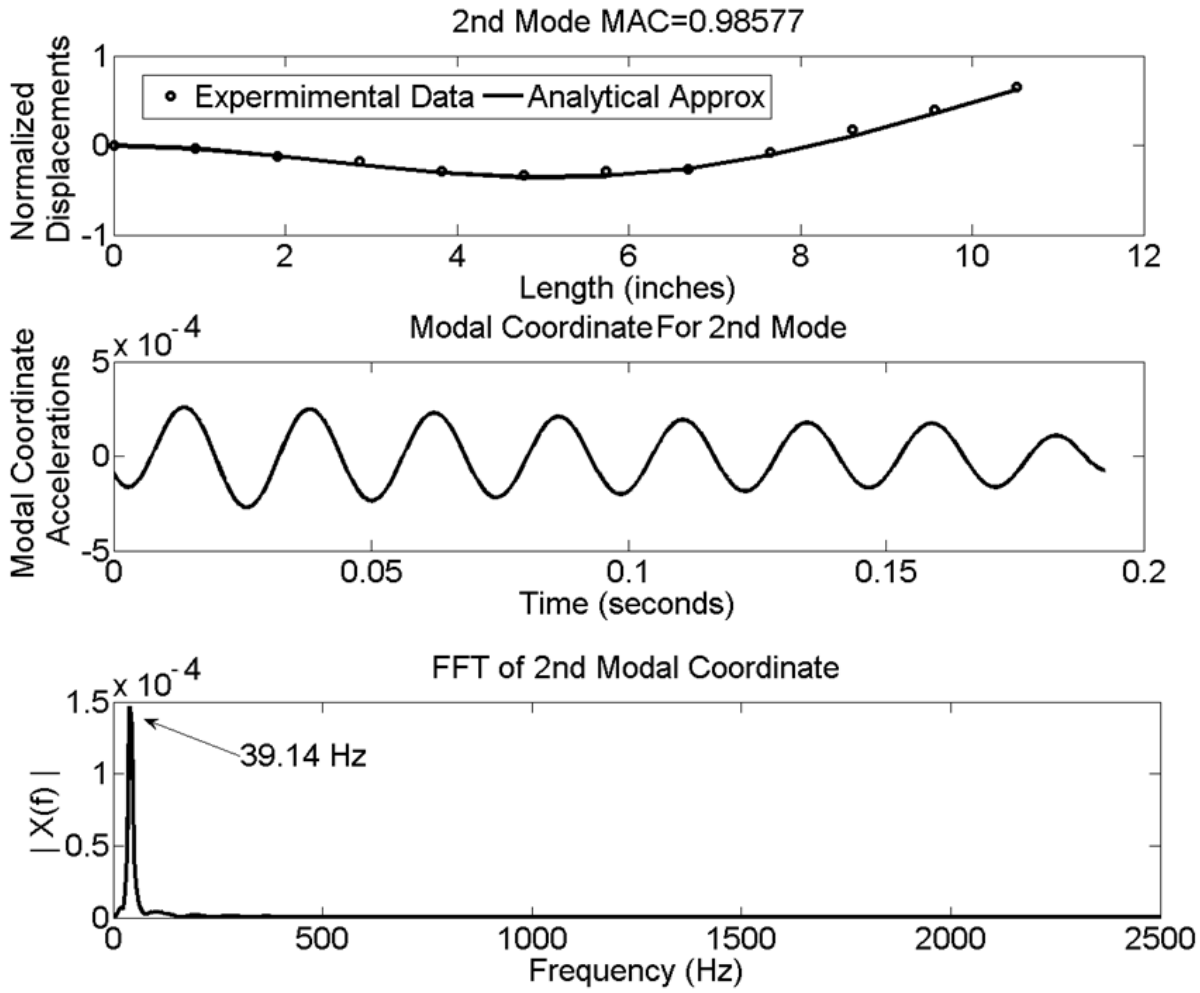

Figure 4.2: Top: second mode shape extracted by RMPOD (o) plotted with the analytical approximation's discretized mode shape (line). Middle: 2nd modal coordinate acceleration from RMPOD. Bottom: fast Fourier transform of modal coordinate acceleration.

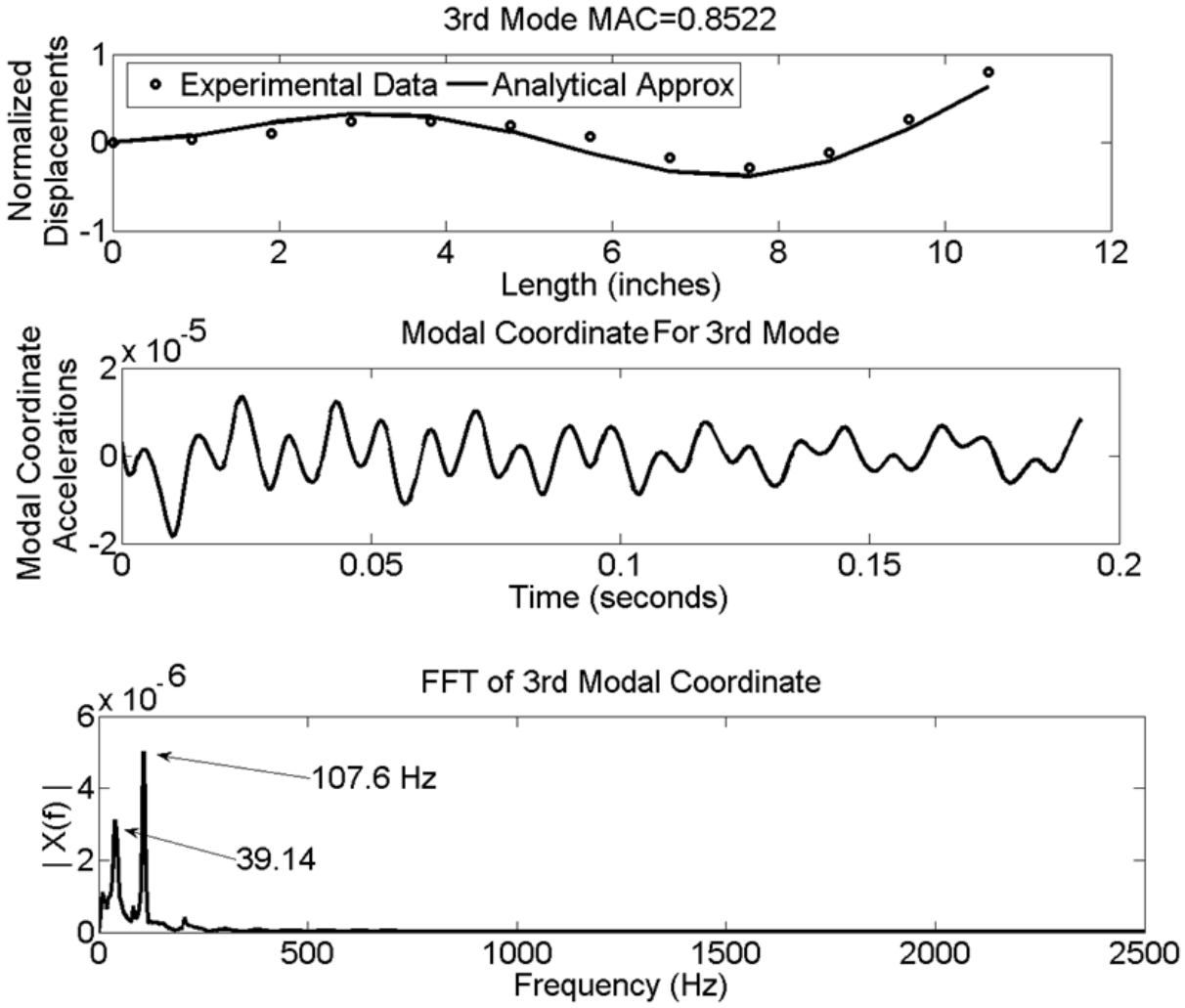

Figure 4.3: Top: third mode shape extracted by RMPOD (o) plotted with the analytical approximation's discretized mode shape (line). Middle: 3rd modal coordinate acceleration from RMPOD. Bottom: fast Fourier transform of modal coordinate acceleration.

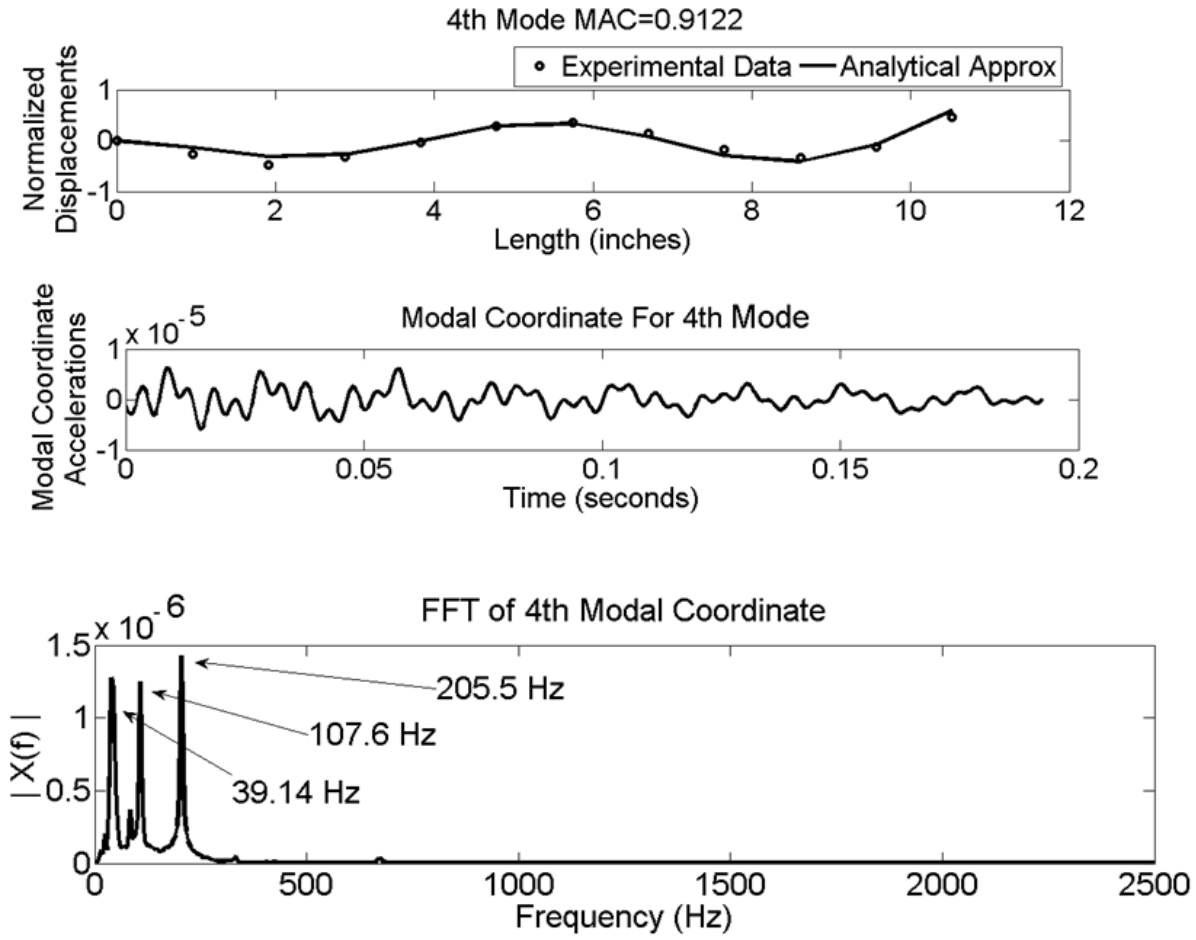

Figure 4.4: Top: fourth mode shape extracted by RMPOD (o) plotted with the analytical approximation's discretized mode shape (line). Middle: 4th modal coordinate acceleration from RMPOD. Bottom: fast Fourier transform of modal coordinate acceleration.

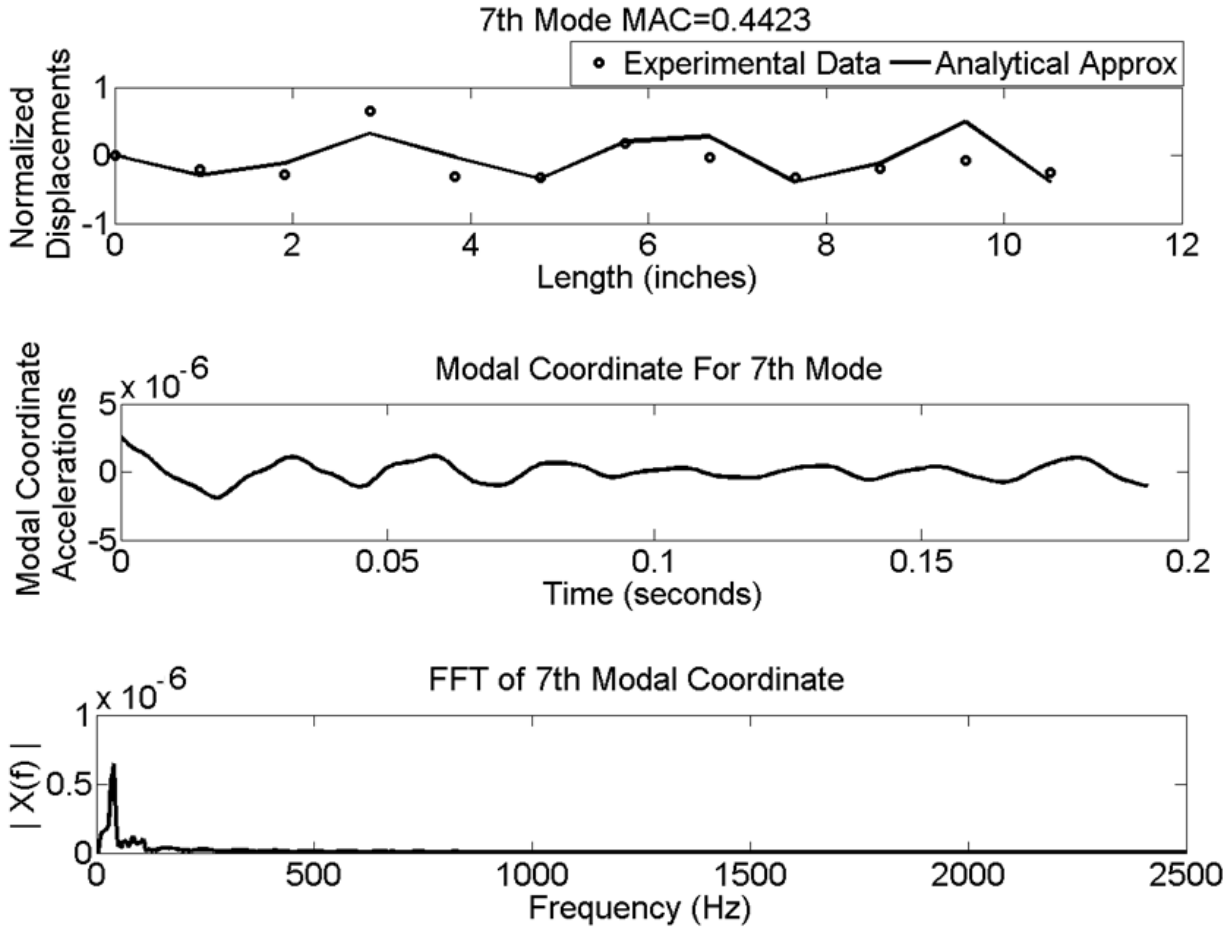

Figure 4.5: Top: seventh mode shape extracted by RMPOD (o) plotted with the analytical approximation's discretized mode shape (line). Middle: 7th modal coordinate acceleration from RMPOD. Bottom: fast Fourier transform of modal coordinate acceleration.

Likewise, ensemble $\mathbf{W} = [\dot{\mathbf{y}}(t_1) \ \cdots \ \dot{\mathbf{y}}(t_N)]$ is setup. In SVMD a $2M \times 2M$ correlation matrix $\mathbf{R}$ is created such that $\mathbf{R} = \dfrac{\mathbf{Y}\mathbf{Y}^T}{N}$. Unique to SVMD, a second $2M \times 2M$ nonsymmetric correlation matrix is created, $\mathbf{N}$, such that $\mathbf{N} = \dfrac{\mathbf{Y}\mathbf{W}^T}{N}$.

POD	SVMD
$\mathbf{X} = [x_1 \ x_2 \ \cdots \ x_M]$	$\mathbf{Y} = \begin{bmatrix} \dot{x_1} \ \dot{x_2} \ \cdots \ \dot{x_M} \\ x_1 \ x_2 \ \cdots \ x_M \end{bmatrix}$
$\mathbf{X} = \begin{bmatrix} x_1(0) & x_1(\Delta T) & \cdots & x_1(M\Delta T) \\ x_2(0) & x_2(\Delta T) & \cdots & x_2(M\Delta T) \\ \vdots & & \ddots & \vdots \\ x_N(0) & x_N(\Delta T) & \cdots & x_N(M\Delta T) \end{bmatrix}$	$\mathbf{Y} = \begin{bmatrix} \dot{x}_1(0) & \dot{x}_1(\Delta T) & \cdots & \dot{x}_1(MT) \\ \dot{x}_2(0) & \dot{x}_2(\Delta T) & \cdots & \dot{x}_2(M\Delta T) \\ \vdots & & \ddots & \vdots \\ \dot{x}_N(0) & \dot{x}_N(\Delta T) & \cdots & \dot{x}_N(M\Delta T) \\ x_1(0) & x_1(\Delta T) & \cdots & x_1(M\Delta T) \\ x_2(0) & x_2(\Delta T) & \cdots & x_2(M\Delta T) \\ \vdots & & \ddots & \vdots \\ x_N(0) & x_N(\Delta T) & \cdots & x_N(M\Delta T) \end{bmatrix}$
$\mathbf{R} = \dfrac{\mathbf{X}\mathbf{X}^T}{N}$	$\mathbf{R} = \dfrac{\mathbf{Y}\mathbf{Y}^T}{N}; \quad \mathbf{N} = \dfrac{\mathbf{Y}\mathbf{W}^T}{N}$
$\mathbf{R}\boldsymbol{\phi} = \lambda\boldsymbol{\phi}$	$\lambda\mathbf{R}\boldsymbol{\phi} = \mathbf{N}\boldsymbol{\phi}$

Table 4.2: POD and SVMD. The first row contains the ensemble matrices. The second row contains the expanded ensemble matrices. The third row contains the correlation matrices. Finally, the last row contains the eigensystem problems.

Once the two correlation matrices are computed, an eigenvalue problem is cast as

$$\lambda\mathbf{R}\boldsymbol{\phi} = \mathbf{N}\boldsymbol{\phi}. \tag{4.2}$$

This problem can be solved for $2M$ eigenvalues, λ, and the eigenvectors $\boldsymbol{\phi}$. If this eigensystem is solved in Matlab using the "eig" command it produces two matrices $\boldsymbol{\Lambda}$ and $\boldsymbol{\Phi}$ corresponding

to eigenvalue problem in matrix form,

$$\mathbf{R\Phi\Lambda} = \mathbf{N\Phi}. \tag{4.3}$$

The eigenvalue matrix $\mathbf{\Lambda}$ is diagonal and contains information about the natural frequencies and, in theory, modal damping. The eigenvector matrix $\mathbf{\Phi}$ contains modal information but the inverse transpose of this matrix must be taken to extract the mode shapes [26]. So the matrix of eigenvectors is $\mathbf{\Psi} = \mathbf{\Phi}^{-T}$ and each $2M \times 1$ column of $\mathbf{\Psi}$ contains information about the mode shapes of the beam. The bottom half of rows $M \times 1$ will contain the mode shapes of the displacements and represent the approximate LNMs. Since the matrix $\mathbf{N}$ is not symmetric the mode shapes may be the complex. If damping is approximately Caughey or Rayleigh (proportional) then the real values of the complex modes approximately correspond to classical linear normal modes. Otherwise, the complex modes correspond to the mode of the state-variable vibration model [27].

4.3.2 Mathematical Development

In this section the mathematical framework for SVMD will be explained. This particular mathematical development was derived in the work of [21] and is meant to provide a description that is easier to follow for the non-specialist. Starting with the basic mass-spring dashpot (MSD) system the governing equation is

$$\mathbf{M\ddot{x}} + \mathbf{C\dot{x}} + \mathbf{Kx} = \mathbf{0} \tag{4.4}$$

where $\mathbf{x}$ and its time derivatives are vectors. Now we can include the following trivial equation in order to transform the system into a state variable one:

$$\mathbf{M}\dot{\mathbf{x}} - \mathbf{M}\dot{\mathbf{x}} = \mathbf{0} \tag{4.5}$$

Writing equations (4.4) and (4.5) together in matrix form leads to the following linear differential equations:

$$\begin{bmatrix} \mathbf{0} & \mathbf{M} \\ \mathbf{M} & \mathbf{C} \end{bmatrix} \begin{bmatrix} \ddot{\mathbf{x}} \\ \dot{\mathbf{x}} \end{bmatrix} + \begin{bmatrix} -\mathbf{M} & \mathbf{0} \\ \mathbf{0} & \mathbf{K} \end{bmatrix} \begin{bmatrix} \dot{\mathbf{x}} \\ \mathbf{x} \end{bmatrix} = \begin{bmatrix} \mathbf{0} \\ \mathbf{0} \end{bmatrix}$$

Now letting

$$\mathbf{y} = \begin{bmatrix} \dot{\mathbf{x}} \\ \\ \mathbf{x} \end{bmatrix} \text{ and } \dot{\mathbf{y}} = \begin{bmatrix} \ddot{\mathbf{x}} \\ \\ \dot{\mathbf{x}} \end{bmatrix}$$

and letting

$$\text{Let } \mathbf{A} = \begin{bmatrix} \mathbf{0} & \mathbf{M} \\ \\ \mathbf{M} & \mathbf{C} \end{bmatrix} \text{ and } \mathbf{B} = \begin{bmatrix} -\mathbf{M} & \mathbf{0} \\ \\ \mathbf{0} & \mathbf{K} \end{bmatrix}$$

leads to

$$\mathbf{A}\dot{\mathbf{y}} + \mathbf{B}\mathbf{y} = \mathbf{0} \tag{4.6}$$

Assuming a solution of the form $\mathbf{y} = \boldsymbol{\phi}\mathbf{e}^{\alpha t}$ yields the eigenvalue problem $\alpha\mathbf{A}\boldsymbol{\phi} + \mathbf{B}\boldsymbol{\phi} = \mathbf{0}$, where α are the eigenvalues, which can be complex. If damping is Caughey, then α has

the form of $\alpha = -\zeta\omega_n \pm \imath\omega_d$ where ω_n is the undamped modal frequency. Zeta, ζ, is the damping coefficient and indicates the peak-to-peak decay rate of the exponential damping envelope. If $\zeta = 0$ then the system is undamped. The frequency of damped oscillation is indicated by $\omega_d = \omega_n\sqrt{1-\zeta^2}$. If $\zeta > 1$ then the system is overdamped, and the α have the form $\alpha = -\zeta\omega_n \pm \omega_n\sqrt{\zeta^2 - 1}$, which are real.

The relationship to the eigensystem problem in equation (4.2) is shown below. Remembering that $\mathbf{R} = \dfrac{\mathbf{Y}\mathbf{Y}^T}{N}$ and $\mathbf{N} = \dfrac{\mathbf{Y}\mathbf{W}^T}{N}$ and substituting into $\alpha\mathbf{R}\boldsymbol{\phi} = \mathbf{N}\boldsymbol{\phi}$ yields $\alpha\mathbf{Y}\mathbf{Y}\boldsymbol{\phi} = \mathbf{Y}\mathbf{W}^T\boldsymbol{\phi}$. Solving (4.6) for $\dot{y}$, and replacing $\dot{y}$ and y with the associated ensembles, W and Y, leads to get $\mathbf{W} = -\mathbf{B}\mathbf{A}^{-1}\mathbf{Y}$. Plugging $\mathbf{W}$ into $\alpha\mathbf{Y}\mathbf{Y}\boldsymbol{\phi} = \mathbf{Y}\mathbf{W}^T\boldsymbol{\phi}$ produces the following sequence of expressions:

$$\begin{aligned}
\alpha\mathbf{Y}\mathbf{Y}^T\boldsymbol{\phi} &= \mathbf{Y} - \mathbf{B}^T\mathbf{A}^{-T}\mathbf{Y}^T\boldsymbol{\phi} \\
\alpha\mathbf{Y}\mathbf{Y}^T\boldsymbol{\phi} &= -\mathbf{Y}\mathbf{B}^T\mathbf{A}^{-T}\mathbf{Y}^T\boldsymbol{\phi} \\
\alpha\mathbf{Y}\mathbf{Y}^T\boldsymbol{\phi} &= -\mathbf{Y}\mathbf{Y}^T\mathbf{B}^T\mathbf{A}^{-T}\boldsymbol{\phi} \\
\mathbf{I}\alpha\boldsymbol{\phi} &= -\mathbf{B}^T\mathbf{A}^{-T}\boldsymbol{\phi}
\end{aligned} \tag{4.7}$$

where α is a scalar and $\boldsymbol{\phi}$ is a vector. The last line was achieved assuming $\mathbf{Y}\mathbf{Y}^T$ is nonsingular and its inverse exists.

Introducing a diagonal matrix $\boldsymbol{\Lambda}$ of eigenvalues α, and a matrix $\boldsymbol{\Phi}$ whose columns are made up of eigenvectors $\boldsymbol{\phi}$, the matrix form of equation (4.7) would be $\boldsymbol{\Phi}\boldsymbol{\Lambda} = -\mathbf{B}^T\mathbf{A}^{-T}\boldsymbol{\Phi}$. Taking the inverse transpose of both sides yields $\boldsymbol{\Phi}^{-T}\boldsymbol{\Lambda}^{-T} = -\mathbf{B}^{-1}\mathbf{A}\boldsymbol{\Phi}^{-T}$. Using the fact that the transpose of a diagonal matrix is the same matrix, letting $\mathbf{U} = \boldsymbol{\Phi}^{-T}$ and

moving some matrices around produces the eigensystem problem $-\mathbf{A}^{-1}\mathbf{B}\mathbf{U} = \mathbf{U}\mathbf{\Lambda}$. The solution of this system will produce is an eigenvalue matrix, $\mathbf{\Gamma}$, and an eigenvector matrix, $\mathbf{\Omega}$, satisfying the equation $-\mathbf{A}^{-1}\mathbf{B}\mathbf{\Omega} = \mathbf{\Omega}\mathbf{\Gamma}$. Comparing the two question together it can be seen that:

$$-\mathbf{A}^{-1}\mathbf{B}\mathbf{\Omega} = \mathbf{\Omega}\mathbf{\Gamma}$$

$$-\mathbf{A}^{-1}\mathbf{B}\mathbf{U} = \mathbf{U}\mathbf{\Lambda}$$

$$\mathbf{U} = \mathbf{\Phi}^{-\mathbf{T}}$$

then

$$\mathbf{\Gamma} = \mathbf{\Lambda}$$

$$\mathbf{\Omega} = \mathbf{\Phi}^{-\mathbf{T}}$$

This is the same result as above where $\mathbf{\Gamma}$ is a diagonal matrix consisting of the $2M$ eigenvalues, and half of complex entries can examined for information on modal frequency and damping. Likewise the bottom half of rows of the $\mathbf{\Omega}$ matrix will yield approximations to linear normal modes.

4.3.3 Experimental Results

SVMD yielded accurate extractions of natural frequencies which corresponded to the FFT of the beam. The natural frequencies extracted by SVMD were 40.08 Hz, 106.42 Hz, and 205.08 Hz for the second, third, and fourth mode, respectively. The FFT of the raw beam acceleration signals produced high magnitude peaks at 40.28 Hz, 107.4 Hz, and 205.5 Hz for the second through fourth modes. These frequencies in addition to other poorly extracted

frequencies are listed in Table 4.6 on page 56.

The SVMD extracted mode shapes showed high similarity to the analytical approximations, as quantified by MAC values near unity as shown in Table 4.4 on page 55. The LNMs predicted by SVMD had MAC values of 0.9921, 0.9729, and 0.9865 for the second, third, and fourth mode respectively. Additional support for this conclusion is shown in Figures 4.7, 4.8, and 4.9. Each plot shows the FFT of the modal coordinates; Figure 4.7 shows a frequency peak at 39.14 Hz for the second mode. In figure 4.8 the third modal coordinate's FFT shows a peak at 107.6 Hz. Finally, Figure 4.9 shows a large peak at 205.5 Hz and a slightly smaller one at 39.14 for the fourth mode. A similar phenomenon was observed for RMPOD. It is also worth noting that the FFT peaks of the modal coordinates are close in value as the SVMD extracted frequencies, and the FFT frequency peaks of the experimental beam accelerations.

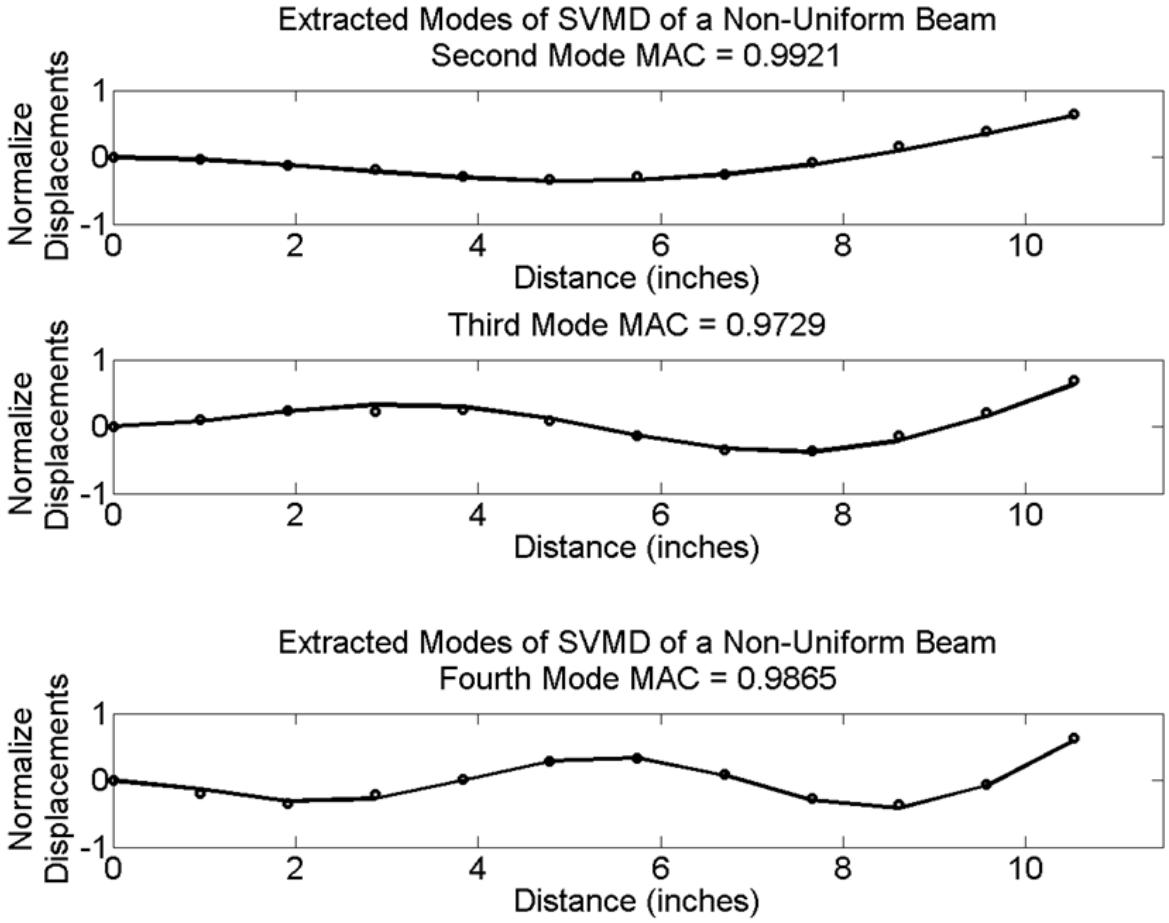

Figure 4.6: The second, third and fourth modes extracted by SVMD.

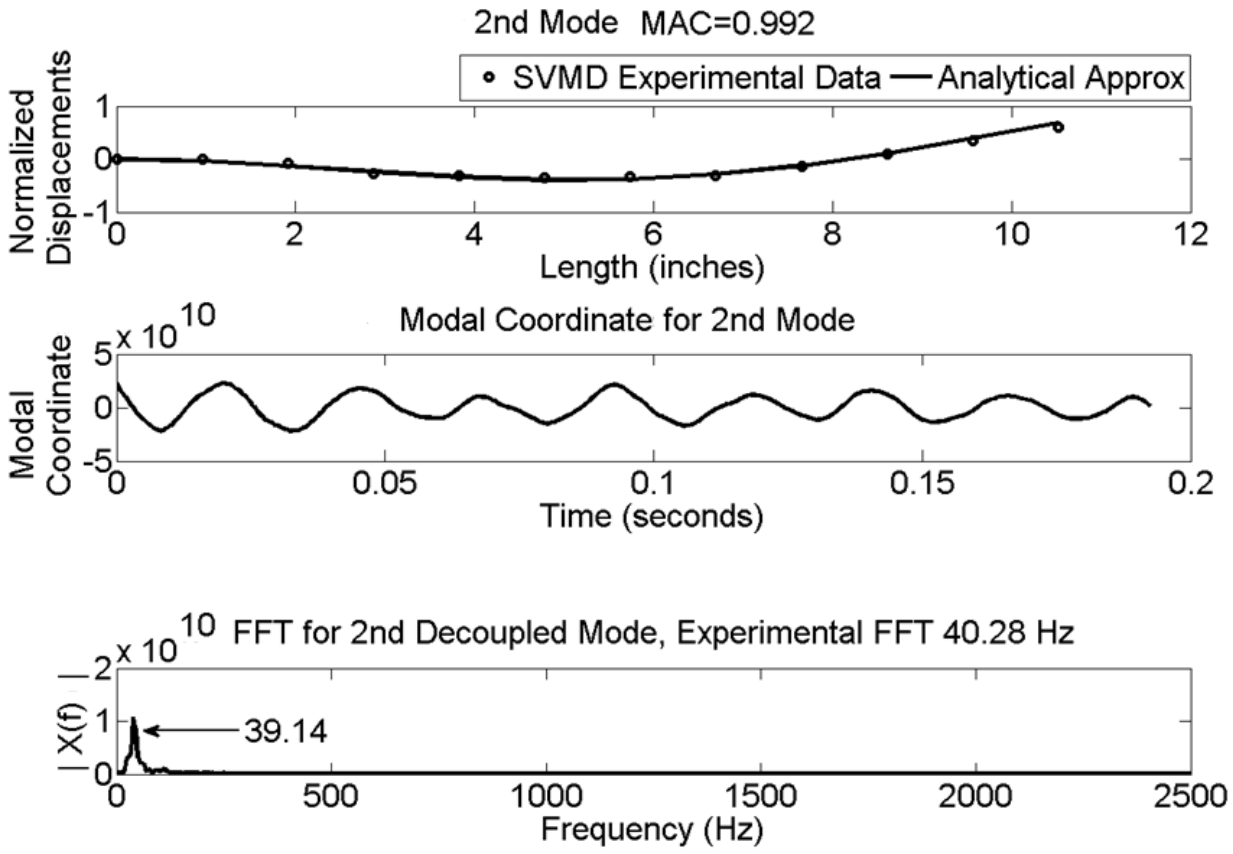

Figure 4.7: Top: second mode shape extracted by SVMD (o) plotted with the analytical approximation's discretized mode shape (line). Middle: second modal coordinate of SVMD. Bottom: fast Fourier transform of the second modal coordinate.

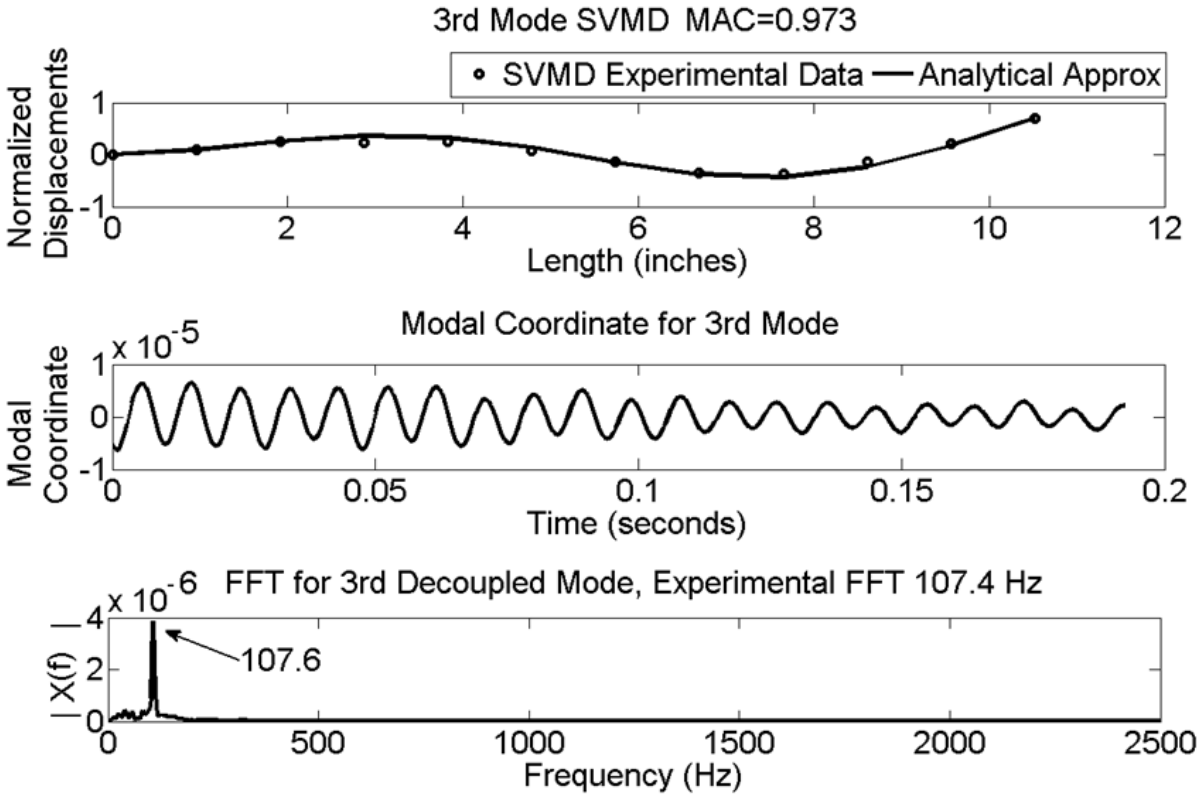

Figure 4.8: Top: third mode shape extracted by SVMD (o) plotted with the analytical approximation's discretized mode shape (line). Middle: third modal coordinate of SVMD. Bottom: fast Fourier transform of the third modal coordinate.

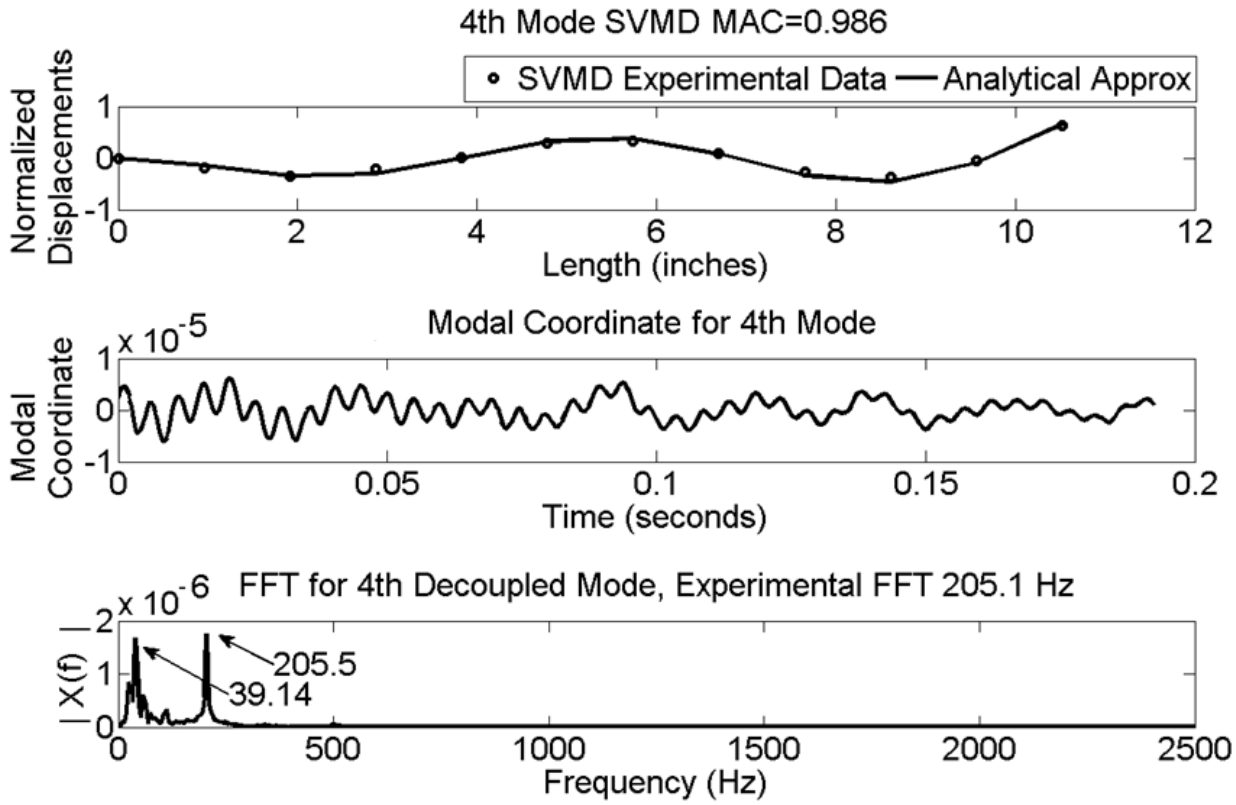

Figure 4.9: Top: fourth mode shape extracted by SVMD (o) plotted with the analytical approximation's discretized mode shape (line). Middle: fourth modal coordinate of SVMD. Bottom: fast Fourier transform of the fourth modal coordinate.

4.3.4 Contribution

Prior works by Feeny and Farooq [28, 26] were conducted on simulations and a uniform beam experiment. In this thesis SVMD was successfully applied to a thin lightly-damped nonuniform beam. As with the previous experiment [26], instead of sensing displacements we sensed accelerations. Using sensed accelerations is computationally easier than using displacements since when using displacements one must use finite differences to get the velocities. As a result of using finite differences great care must be taken to make sure the resulting velocity and displacement ensemble matrices are dimensionally compatible. A concern with using finite differences is that it magnifies high frequency noise. The power in the SVMD lies in the fact that a mass matrix is not needed for nonuniform structures, which is the case with MWPOD. Input measurements are also not needed. Moreover, without needing the mass matrix, SVMD enables the practitioner to extract approximations to the LNMs, natural frequencies, and possibly modal damping coefficients.

4.4 Smooth Orthogonal Decomposition

4.4.1 Background

Smooth orthogonal decomposition (SOD) is another generalization of POD [17]. Like POD, MWPOD, and SVMD, SOD uses sensed outputs, normally velocity and displacement, to extract the natural frequencies and approximations to LNMs. Like all of the decomposition methods discussed in this thesis, ensemble matrices of measurements are created. In the case of SOD two correlation matrices are created. One is the displacement correlation matrix $\mathbf{R}$,

such that $\mathbf{R} = \dfrac{\mathbf{X}\mathbf{X}^T}{N}$, and the other is the velocity correlation matrix $\mathbf{S} = \dfrac{\mathbf{V}\mathbf{V}^T}{N}$, where $\mathbf{V}$ is an ensemble of velocity measurements. $\mathbf{R}$ and $\mathbf{S}$ must be the same dimensions. Next, $\mathbf{R}$ and $\mathbf{S}$ are used in the generalized eigenvalue problem described by $\lambda\mathbf{R}\boldsymbol{\psi} = \mathbf{S}\boldsymbol{\psi}$. The eigenvalues approximate (in theory) the squares of the modal frequencies, such that $\omega_n = \sqrt{\lambda}$, and LMNs are approximated by columns of $\boldsymbol{\Phi} = \boldsymbol{\Psi}^{-T}$, where $\boldsymbol{\Psi}$ is a matrix whose columns are eigenvectors of the generalized eigenvalue problem.

In application, SOD has been shown to extract approximations to LNMs and natural frequencies from simulated discrete and continuous systems [17]. In the work by Chelidze and Zhou [17] it was shown that SOD can extract modal information from the superposition of sinusoids of the same amplitude but different frequencies, i.e, $x_k = \sin 2\pi f_k t$, which points out one of the benefits of SOD over POD since POD fails to extract LNM in this particular case. However such "real world" situations of this case may be rare. Other case studies performed by Chelidze and Zhou [17] are shown in the Table 4.3. Additionally, Chelidze and Zhou showed that SOD can extract modal information from damped free vibrating systems and modal information of forced damped system if the system is forced at a resonance.

Case	POD	SOD
Same amplitude, different frequencies	×	✓
Different amplitude, different frequencies	✓	✓
Different amplitude, same frequencies	✓(largest amplitude)	×

Table 4.3: SOD vs POD case study.

4.4.2 Mathematical Development

The relationship between the SOD EVP and the general mass-spring system with negligible damping can be shown following the development in [29]. The vibration system can be

written as $\mathbf{M}\ddot{\mathbf{x}}+\mathbf{K}\mathbf{x}=\mathbf{0}$. As shown in prior sections this reduces to the following eigenvalue problem: $-\omega\mathbf{M}\boldsymbol{\phi}+\mathbf{K}\boldsymbol{\phi}=\mathbf{0}$. If we create a modal matrix of eigenvectors and a diagonal matrix of eigenvalues then this can be written as

$$\mathbf{K}\boldsymbol{\Phi}=\mathbf{M}\boldsymbol{\Phi}\boldsymbol{\Lambda}. \tag{4.8}$$

Remembering that SOD is an eigenvalue problem described as $\lambda\mathbf{R}\boldsymbol{\psi}=\mathbf{S}\boldsymbol{\psi}$ and that $\mathbf{R}=\frac{\mathbf{X}\mathbf{X}^T}{N}$, $\mathbf{S}=\frac{\mathbf{V}\mathbf{V}^T}{N}$, and $\mathbf{V}\cong\mathbf{X}\mathbf{D}^T$, where $\mathbf{D}$ is a finite difference matrix operator, we can rewrite the SOD eigenvalue problem as

$$\lambda\frac{\mathbf{X}\mathbf{X}^T}{N}\boldsymbol{\psi}=\frac{\mathbf{X}\mathbf{D}^T\mathbf{D}\mathbf{X}^T}{N}\boldsymbol{\psi}.$$

Using $\mathbf{D}^T\mathbf{D}\mathbf{X}^T\approx-\mathbf{A}^T$, where $\mathbf{A}$ is an ensemble of sampled accelerations,$\ddot{\mathbf{x}}$, and noting $\mathbf{A}=-\mathbf{M}^{-1}\mathbf{K}\mathbf{X}$ [17] (i.e. solving $\mathbf{M}\ddot{\mathbf{x}}+\mathbf{K}\mathbf{x}=\mathbf{0}$ for $\ddot{\mathbf{x}}$); we arrive at

$$\lambda\mathbf{X}\mathbf{X}^T\boldsymbol{\psi}=-\mathbf{X}\mathbf{X}^T\mathbf{K}\mathbf{M}^{-1}\boldsymbol{\psi}.$$

Assuming that the determinant of $\mathbf{X}\mathbf{X}^{\mathrm{T}}$ is not equal to zero and is thus invertible, then we can simplify the previous equation to $\lambda\boldsymbol{\psi}=-\mathbf{K}\mathbf{M}^{-1}\boldsymbol{\psi}$. Creating matrices of the eigenvectors and eigenvalues we can write this in matrix form as $\boldsymbol{\Psi}^{-\mathrm{T}}\boldsymbol{\Lambda}^{-1}=\mathbf{K}^{-1}\mathbf{M}\boldsymbol{\Psi}^{-\mathrm{T}}$. Moving $\mathbf{K}$ so that it is not inverted we arrive at

$$\mathbf{K}\boldsymbol{\Psi}^{-\mathrm{T}}=\mathbf{M}\boldsymbol{\Psi}^{-\mathrm{T}}\boldsymbol{\Lambda}.$$

If we compare this equation to equation (4.8) it can be seen that $\mathbf{\Phi} = \mathbf{\Psi}^{-\mathrm{T}}$. Therefore the inverse transpose of the eigenvector matrix of $\lambda\mathbf{R}\boldsymbol{\psi} = \mathbf{S}\boldsymbol{\psi}$ produces a modal matrix whose columns approximate the LNMs.

4.4.3 Experimental Results

The results suggest that SOD can extract approximations to the LNMs as illustrated by MAC values close to unity [25]. The corresponding time histories were divided up into several time windows in order to extract modal information without pollution from other modes. The biggest restraint was having a sufficient number of cycles for modes with low natural frequencies. The natural frequencies for the second, third, and fourth modes of the experimental beam via FFT are 40.28 Hz, 107.4 Hz, and 205.1 Hz respectively. The natural frequencies predicted by SOD are these modes are 43.72 Hz, 107.77 Hz, and 203.53 Hz. These frequencies in addition to other poorly extracted frequencies are listed in Table 4.6 on page 56. The SOD predicted mode shapes which, when compared to the discretized analytical mode shapes had MAC valves of 0.999, 0.820, and 0.937. From these results it can be concluded that the SOD can extract the lower modes of a lightly-damped nonuniform cantilevered beam. Figures 4.10, 4.11, 4.12 shows the SOD extracted modes for the 2nd, 3rd, and 4th modes respectively. These modes are plotted with the discretized analytical approximations of a nonuniform Euler-Bernoulli beam.

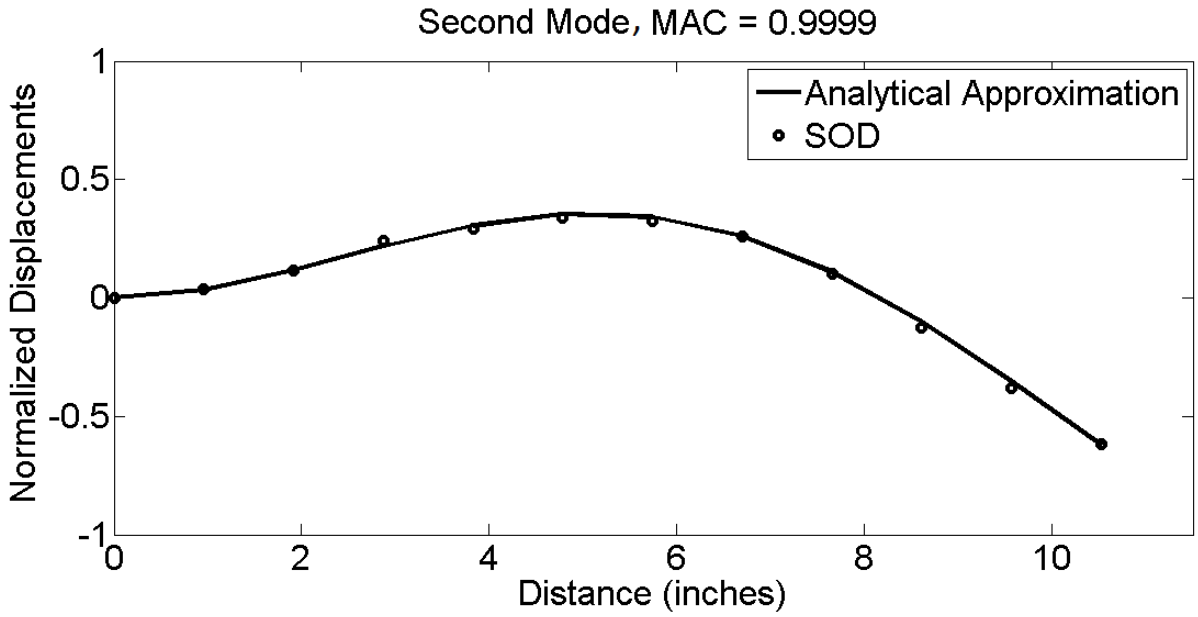

Figure 4.10: SOD extracted second mode (o) compared to the analytical approximation (solid line).

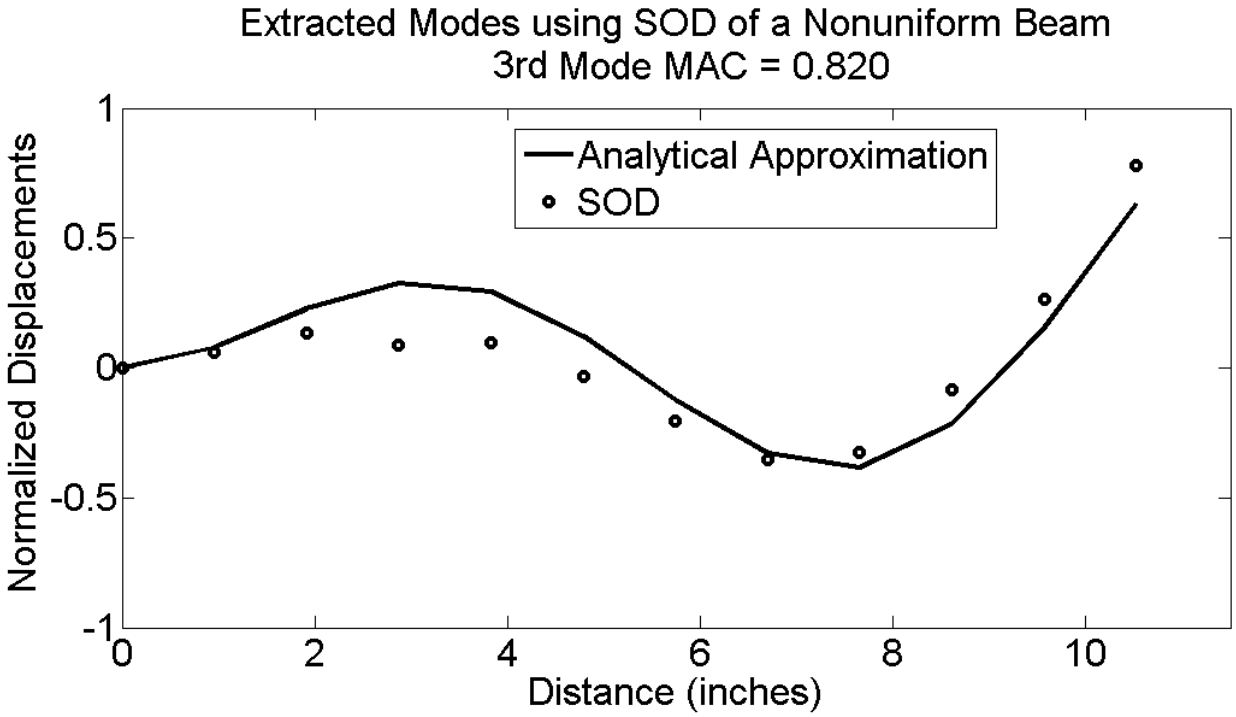

Figure 4.11: SOD extracted third mode (o) compared to the analytical approximation (solid line).

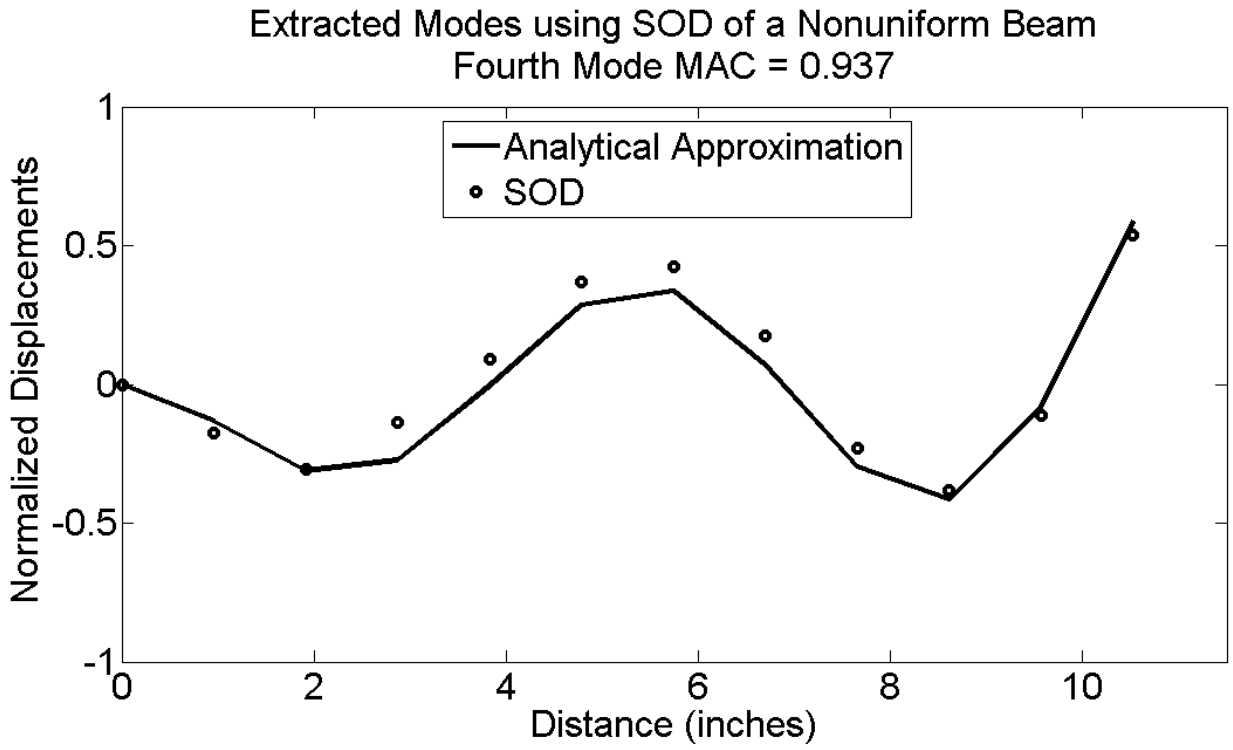

Figure 4.12: SOD extracted fourth mode- (o) compared to the analytical approximation (solid line).

4.4.4 Contribution

Chelidze and Zhou [17], did extensive simulations comparing SOD to POD. In these simulations they studied the applicability of SOD to extracted modal information from outputs consisting of the sum of sinusoids which had the same amplitude and different frequencies, different amplitudes and different frequencies, and finally, different amplitudes and same frequencies. Additional studies included damped vibrations and forced oscillations. These were performed on discrete systems and distributed parameter systems. Farooq and Feeny used SOD to extract the modal information from and simulated randomly excited lightly damped discrete system [29].

This work contributes to the field first by using experimental data and not simulations

and second by using a nonuniform beam. This research has shown that it is possible to extract modal information from a lightly-damped freely vibrating nonuniform cantilevered beam. The experimental results was compared with an analytical approximation of an Euler-Bernoulli beam.

4.5 Method Comparison

As a final cross-check, each method was compared to each other using MAC as shown in the Tables 4.4 and 4.5 below. The tables show a strong similarity between each method. Table 4.6 shows the extracted frequencies for SVMD and SOD. It looks like in this experiment all methods were successful for extracting their respective modal parameters for the lower modes. Table 4.7 lists some of the benefits and drawbacks of each method. However, the drawbacks of each decomposition method are not serious.

Modes	RMPOD	POD	SVMD	SOD
2	0.986	0.982	0.992	0.999
3	0.852	0.829	0.973	0.820
4	0.912	0.585	0.986	0.937
5	0.915	0.746	0.961	0.680
6	0.861	0.430	0.081	0.054

Table 4.4: MAC values for decomposition methods when compared to the discretized analytical analysis mode shapes.

Modes	RMPOD vs SOD	RMPOD vs SVMD	SOD vs SVMD
2	0.9893	0.9702	0.9926
3	0.8027	0.8751	0.9138
4	0.8907	0.9214	0.9507
5	0.5255	0.8728	0.8263
6	0.0023	-	-

Table 4.5: Cross comparison of decomposition methods using MAC values.

mode	SVMD	SOD	FFT
2	40.08 Hz	43.72 Hz	40.28 Hz
3	106.42 Hz	107.77 Hz	107.4 Hz
4	205.08 Hz	203.53 Hz	205.1 Hz
5	306.04	291.38 Hz	498.0 Hz
6	480.75	446.72 Hz	677.3 Hz

Table 4.6: SVMD and SOD extracted frequencies.

RMPOD	
PROS	CONS
can estimate mode shapes RMPOVs estimate modal strength requires single **R** requires **X** only input signal not needed	frequencies not directly estimated (need **Q**) need to compute the reduced mass matrix
SVMD	
can estimate mode shapes estimate modal frequencies directly possibility of modal damping directly mass not required input signal not needed	no modal strength, except by **Q** need **X**, **V**, and **A**
SOD	
can estimate mode shapes estimate modal frequency directly mass not required input signal not needed	no modal strength except by **Q** need **X** and **V**

Table 4.7: Pros and cons of each decomposition method.

Chapter 5

Conclusions

All results shown in this thesis used the following input parameters: a small impulse (as defined in Chapter Two), the beam was struck at $x = 2$ inches, and a sample window of $t = [1/4L_S\ 1/2L_S]$ where L_S is the signal length.

Three decomposition methods were applied to the output-only modal analysis of a nonuniform beam experiment whose modal frequencies were 8.454 Hz, 40.28 Hz, 107.4 Hz, 205.1 Hz, 498 Hz, and 677.3 Hz obtained by fast Fourier transform. The first mode was filtered out since it was below the range of reliable accelerometer performance. The beam was modeled as a nonuniform Euler-Bernoulli beam. An analytical approximation for the mode shapes was developed and the predicted mode shapes and natural frequencies were compared to the results from modal decomposition of the experimental beam. The natural frequencies predicted by the model were proportionally consistent with those identified experimentally, and could therefore be used to identify a parameter group.

The reduced-order mass-weighted POD was applied under a permutation of conditions involving impulse location and strength, and using decompositions based on displacement,

velocity and acceleration signals. RMPOD extracted good approximations to the 2nd, 3rd, and 4th LNMs as suggested by near unit MAC values between the extracted modes and the analytical approximations of the modes. Those values were 0.986, 0.852, and 0.912 for the second, third, and fourth mode, respectively, when accelerations were used as the output and a small impulse was applied two inches from the clamp. Further confirmation on the quality of the modes was provided from computing the modal coordinates and taking their FFTs. The peak frequency for the lowest extracted mode was dominant. For increasingly higher modal coordinates, frequencies of other modes leaked in from other modes. The pollution of these modes had little effect on the approximation to the LNMs.

SVMD and SOD were also employed to extract approximations of the natural modal frequencies and approximations to the LNMs. SVMD extracted natural frequency approximations that were 40.08 Hz, 106.42 Hz, and 205.08 Hz for the second, third, and fourth mode, respectively. The MAC values for these modes when compared to the analytical approximations were 0.9921, 0.9729, and 0.9865. SOD predicted frequencies of 43.72 Hz, 107.77 Hz, and 203.53 Hz. The predicted mode shapes had MAC values of 0.986, 0.984, and 0.989.

This work contributes to ongoing research on output-only modal decomposition methods as the first application of RMPOD and SOD to a modal analysis experiment, and as the first application of SVMD to an inhomogeneous experiment, thereby supporting the feasibility of these methods. These tests suggest that RMPOD, SVMD, and SOD can be reliable methods of modal analysis, at least for the lower modes of a structure. These methods are easy to apply. The necessary signal processing was in integrating the accelerometer signals into the desired quantify (displacement, velocity or acceleration), with high pass filtering used to prevent integrator drift. Application of the methods in concert can be useful in confirming

results.

BIBLIOGRAPHY

BIBLIOGRAPHY

[1] W.T. Thomson and M.D. Dahleh. *Theory of Vibration with Application 5th Edition*. Prentic-Hall, 1998.

[2] Enrico Volterra and E.C. Zachmanoglou. *Dynamics of Vibrations*. Charles E. Merrill Books, Inc., Columbus, Ohio, 1965.

[3] K. Yusuf Bilah and Robert Scanlan. Resonance, tacoma narrows bridge failure, and undergraduate physics textbooks. *American Journal of Physics*, 59 (2):118–124, 1991.

[4] J. M. T. Thompson and H. B. Stewart. *Nonlinear Dynamics and Chaos*. John Wiley, Chichester, 1986.

[5] D. J. Inman. *Engineering Vibration*. Prentice-Hall, 1996.

[6] Peter Avitabile. Experimental modal analysis; a simple non-mathematical presentation. *Sound and Vibration*, 32(1):20–31, January 2001.

[7] U. Farooq and B. F. Feeny. Smooth orthogonal decomposition for modal analysis of randomly excited systems. *Journal of Sound and Vibration*, 316(1-5):137 – 146, 2008.

[8] J.N. Juang and R. Pappa. An eigensystem realization algorithm for modal parameter identification and model reduction. *Journal of Guidance, Control and Dynamics*, 8 (5):620627, 1985.

[9] S.R. Ibrahim and E.C. Mikulcik. A method for the direct identification of vibration parameters from the free response. *Shock and Vibration Bulletin*, 47 (4):183–198, 1977.

[10] G. Kerschen, F. Poncelet, and J.C. Golinval. Physical interpretation of independent component analysis in structural dynamics. *Mechanical Systems and Signal Processing*, 21 (4):15611575, 2007.

[11] F. Poncelet, G. Kerschen, J.C. Golinva, and D. Verhelst. Output-only modal analysis using blind source separation techniques. *Mechanical Systems and Signal Processing*, 21:pp. 23352358, 2007.

[12] H. Vold, J. Kundrat, G. Rocklin, and R. Russel. A multi-input modal estimation algorithm for mini-computer. *SAE Technical Papers Series*, 91:815821, 1982.

[13] H. Vold. Orthogonal polynomials in the polyreference method. In *Katholieke University of Leuven, Belgium*. Katholieke University of Leuven, Belgium, 1986.

[14] M. Richardson and D. L. Formenti. Parameter estimation from frequency response measurements using rational fraction polynomials. In *Proceedings of the International Modal Analysis Conference*, pages 167–182.

[15] C.Y. Shih, Y.G. Tsuei, R.J. Allemang, and D.L. Brown. Complex mode indication function and its application to spatial domain parameter estimation. *Mechanical System and Signal Processing*, 2:367–377, 1988.

[16] R. Brincker, L. Zhang, and P. Andersen. Modal identification of output-only systems using frequency domain decomposition. *Smart Materials and Structures*, 10:441445, 2001.

[17] D. Chelidze and W. Zhou. Smooth orthogonal decomposition-based vibration mode identification. *Journal of Sound and Vibration*, 292:461–473, 2006.

[18] V. K. Yadalam and B. F. Feeny. Reduced mass weighted proper decomposition for modal analysis. *Journal of Vibration and Acoustics*, 133(2):024504, 2011.

[19] J. Hass G. Thomas Jr, M. Weir and F. Giordano. *Thomas' Calculus*. Pearson- Addison Wesley, 2008.

[20] S. R. Ibrahim and E. C. Mikulcik. A method for the direct identification of vibration parameters from the free response. *Shock and Vibration Bulletin*, 47(4):183–198, 1977.

[21] Umar Farooq. *Orthogonal Decomposition Methods for Modal Analysis*. PhD thesis, Michgian State University, 2009.

[22] A. Chatterjee. An introduction to the proper orthogonal decomposition. *Current Science*, 78 (7):808–817, April 2000.

[23] G. Berkooz, P. Holmes, and J. L. Lumley. The proper orthogonal decomposition in the analysis of turbulent flows. *Annual reviews of Fluid mechanics*, 25:539–575, 1993.

[24] B. F. Feeny and R. Kappagantu. On the physical interpretation of proper orthogonal modes in vibrations. *Journal of Sound and Vibration*, 211(4):607 – 616, 1998.

[25] R.A. Allemang. The modal assurance criterion (MAC): Twenty years of use and abuse. *Sound and Vibration*, August:14–21, 2003.

[26] B. F. Feeny and U. Farooq. A nonsymmetric state-variable decomposition for modal analysis. *Journal of Sound and Vibration*, 310(4-5):792–800, March 2008.

[27] L. Meirovitch. *Principles and Techniques of Vibrations*. Prentice Hall, NewYork, 1997.

[28] B. F. Feeny and U. Farooq. A state-variable decomposition method for estimating modal parameters. In *ASME International Design Engineering Technical Conferences*, Sep 2007.

[29] U. Farooq and B. F. Feeny. Smooth orthogonal decomposition for randomly excited systems. *Journal of Sound and Vibration*, 316(3-5):137–146, Sep 2008.